COO-2263-15
NSR 2-15

RASOR ASSOCIATES, INC.

ADVANCED THERMIONIC ENERGY CONVERSION

DOE CONTRACT EY-76-C-02-2263

JPL CONTRACT 955033

JOINT HIGHLIGHTS AND STATUS REPORT

APRIL - JUNE 1979

PREPARED BY

RASOR ASSOCIATES, INCORPORATED
253 HUMBOLDT COURT
SUNNYVALE, CALIFORNIA 94086

TABLE OF CONTENTS

		Page
INTRODUCTION AND SUMMARY		
RELEVANT PUBLICATIONS AND PRESENTATIONS IN 1978 AND 1979		
PART I - DOE PROGRAM		
TASK 1 - THERMIONIC CONVERTER RESEARCH AND TECHNOLOGY		1
1.1.1	THX Converter Development (L. L. Begg, M. L. Manda, B. Carlsmith, M. Smith)	1
1.1.2	Heat Transfer Technology (L. L. Begg, D. Johnson)	9
1.1.3	System Analysis (G. O. Fitzpatrick, E. J. Britt)	13
1.2.1	Converter Technology (M. L. Manda, N. S. Rasor)	14
1.3.1	Converter Performance Analysis (E. J. Britt, J. McVey)	23
1.3.2	Plasma Characterization (G. L. Hatch)	36
1.3.3	Electrode Surface Characterization (J.-L. Desplat, L. K. Hansen, H. Woo)	36
1.3.4	Thermionic Converter Data Review (L. K. Hansen)	44
TASK 2 - THX POWER MODULE EVALUATION		
2.1.1	THX Test Module (L. L. Begg, B. Carlsmith)	44
2.1.2	Heat Source (L. L. Begg, D. Johnson)	45
2.1.3	Output Power Transfer System (L. L. Begg, E. J. Britt)	45
2.1.4	Heat Transfer System (L. L. Begg)	51
2.2	Conceptual Plant Design (G. O. Fitzpatrick, E. J. Britt)	51
PART II - NASA/JPL PROGRAM		
TASK 1 - CONVERTER FABRICATION AND TEST (G. L. Hatch, M. L. Manda)		54
TASK 2 - UNINSULATED HEAT PIPE THERMIONIC POWER ANALYSIS (E. J. Britt)		55
REFERENCES		56
APPENDIX 1: THE AUXILIARY ION SOURCE ANALYTICAL MODEL "AIS-1"		

INTRODUCTION AND SUMMARY

The ADVANCED THERMIONIC ENERGY Conversion Program at Rasor Associates, Inc. is supported by U.S.Department of energy and the National Aeronautics and Space Administration through the Jet Propulsion Laboratory.

The DOE portion of the effort is directed primarily toward terrestrial applications of thermionic energy conversion. It focuses on the development of converters suitable for use with fossil fueled heat sources in power plants. Studies have shown that the successful use of thermionic power modules in coal-fired central station power plants, for example, could improve plant efficiencies from their current average level of 33% to 50% or more. Such an improvement would provide a fuel savings of over 25% while cutting waste heat in half. The objective of the program is to develop such modules in the mid-1980's for commercial applications in the late 1980's and early 1990's.

The NASA program is directed at establishing the technical feasibility of an advanced light-weight long-life thermionic conversion system compatible with a remote nuclear or solar heat source. The principal application forseen at this time is in nuclear electric propulsion (NEP) missions in the mid-1990's.

Both sponsors cooperate in the improvement of converter performance. In addition, the DOE effort includes the evaluations of a preprototype Thermionic Heat Exchanger (THX) designed for central station power plant applications and NASA/JPL is supporting a study of thermionic NEP systems performance as a function of converter performance and design.

This report covers progress made during the three month period from April 1, 1979 through June 30, 1979.

Significant accomplishments for the three month period include:

DOE Program:

- Devised a blade-type distributed lead design with many advantages compared to the stud-type distributed lead
- Completed design of Marchuk tube test apparatus

- Concluded, based on current understanding, that residual hydrogen should not contribute to a negative space charge barrier at the collector
- Modified THX design program to include series-coupled designs as well as inductively-coupled designs
- Initiated work on the Heat Transfer Technology (1.1.2), THX Test Module (2.1.1), Output Power Transfer System (2.1.3), Heat Transfer System (2.1.4), and Conceptual Plant Design (2.2) tasks

NASA Program:

- Reached 2200 hours of operation in JPL-5 cylindrical converter envelope test

RELEVANT PUBLICATIONS AND PRESENTATIONS IN 1978 AND 1979

1. "Thermionics and its Application to the SPS" presented at the 3rd Radiation Energy Conversion Conference, 1/78, published in Radiation Energy Conversion in Space, Vol. 61 of Progress in Astronautics and Aeronautics, K. W. Billman editor

2. "Thermionic Energy Conversion for Solar Applications" presented at the STTF Users Meeting, 4/78

3. "Analytical Model for Auxiliary Ion Source Thermionic Converters" presented at the Int. Conference on Plasma Science, 5/78

4. "Negative Ion Emission from Cesiated Electrodes" presented at the Int. Conference on Plasma Science, 5/78

5. "Advanced Thermionic Energy Conversion" Biennial Report for Period 9/75 - 9/77, NSR 2-7, COO-2263-7 Sept. 1, 1975 - Sept. 30, 1977 (2 volumes)

6. "A Summary of USSR Thermionic Energy Conversion Activity," N. S. Rasor, presented at the IECEC, 8/78

7. "Thermionic Power Plant Design Point Selection: The Economic Impact," G. O. Fitzpatrick and E. J. Britt, presented at the IECEC, 1978

8. "Analytical Model for the Ignited Mode Thermionic Converter," L. K. Hansen, J. B. McVey, and E. J. Britt, NSR 2-8, COO-2263-8 Aug. 1978

9. "Negative Ions and the Collector Sheath," L. K. Hansen, NSR 2-9, COO-2263-9 August 1978

10. "High Current Thermionic Converter Test Facility, and Initial Converter Test Results," G. O. Fitzpatrick and L. L. Begg, NSR 2-10, COO-2263-10 Sept. 1978

11. "Thermionic Converters and Low-Temperature Plasma," edited by L. K. Hansen, DOE-tr-1, Baksht et.al. April 1978

12. "Analysis of Advanced Thermionic Converters," J. McVey, L. K. Hansen, and E. J. Britt, presented at the IEEE Plasma Science Conference, 6/79

13. "Emission and Space Charge Effects at Cesiated Electrodes," L. K. Hansen and H. Y. Woo, presented at the IEEE Plasma Science Conference, 6/79

14. "Low Cost Cylindrical Converters for Measuring Lead Efficiency," G. L. Hatch, L. Nakata, and E. J. Britt, presented at the IECEC, 8/79

15. "Power Coupling Alternatives for the NEP Thermionic Power System," M. L. Manda, E. J. Britt, G. O. Fitzpatrick, NSR 7-1, JPL Contract 955121 12/78

16. "A Study of Cesium Oxygen Coadsorption on Metallic Substrates," J.-L. Desplat, NSR 6-2, NASA CR-152272 5/79. To be published as two papers in Surface Science, Vol. 91, 1980.

17. "Experimental and Analytical Study of an Advanced Mode Thermionic Converter," G. L. Hatch, L. K. Hansen, and E. J. Britt, NSR 5-2, NASA CR-159638 6/79

18. "A Clean Source of Metallic Zr for Ultrahigh Vacuum Surface Studies," P. R. Davis and H. R. Poppa, J. of Vac. Sci. and Technology, 15, 1771, 1978

19. "The Adsorption of Zr Onto W(100) Surfaces," to be published in Surface Science, Vol. 91, 1980

20. "A Study of Zirconium-Oxygen Coadsorption on Single Crystal Tungsten Surfaces," Paul R. Davis, Final Report NAS2-9629 5/78

21. "ZEPO" - The Worlds Largest Thermionic Converter," L. L. Begg and G. O. Fitzpatrick, presented at the 14th IECEC, 8/79

PART I - DOE PROGRAM

TASK 1 - THERMIONIC CONVERTER RESEARCH AND TECHNOLOGY

1.1.1 THX Converter Development (L. L. Begg, M. L. Manda, B. Carlsmith, M. Smith)

Introduction: The objective of this task is to develop cost effective, reliable, and reproducible converter configurations which can effectively interface with other thermionic power module components. The terrestrial applications for thermionic energy conversion put tight constraints on conversion system costs and operating characteristics, such as part load efficiency, load following capability, start up power requirements, etc. However, constraints on system size and weight are of lesser importance. As a result, new innovations in converter design and operation such as the use of high current, all metal seals, distributed leads, and inductive output power coupling can significantly improve system operational characteristics and reduce costs. The THX power module has been designed to take full advantage of these innovations. To demonstrate their advantages requires detailed analysis and testing of each new design concept to establish both its viability and its impact on the system performance and operation. To accomplish this, a High Current Converter Test Facility has been built to test a series of high current (HC) converters which will sequentially incorporate and demonstrate each advance in design. The test last year of HC-1, (ZEPO), the first converter in the series, demonstrated the basic feasibility of large converters by stably driving a uniform current exceeding 6500 amperes.[1] The feasibility of using inductive power coupling was demonstrated using a "mini-system" which incorporated a small converter (A_E ~10 cm^2), operating in air.[2] The converter provided sufficient power while operating in the flux-reset inductive power coupling mode to drive all the circuitry required for operating in addition to a light bulb load bank.

Work during this contract period is concentrating on two attractive approaches for improving THX performance while reducing cost.

First, the characteristics of a small-scale, bolt-together "Cold Seal" converter will be determined experimentally. In this concept, a low pressure (~1 torr) of inert gas is introduced into the interelectrode space. During operation, the cesium vapor displaces the inert gas to the end of the converter as in a "gas-buffered" heat pipe, establishing a cesium-free, inert-gas buffer space. Since no cesium is present in this region, it can be below the cesium reservoir temperature, permitting the use of low-temperature, easily-replaced seals. This, in turn, may permit rapid and inexpensive assembly and disassembly of the converter as well as reduced seal costs. Second, the materials and joint designs which will be used in distributed leads will be tested. Based on the results of this work, a second high current converter, HC-2, will be designed, built, and tested to evaluate these concepts at the THX scale. HC-2, will be designed and built to deliver current to an external load, permitting acquisition of current-voltage data and information on dynamic operating characteristics.

Current Effort:

Cold Seal Converter (M. L. Manda, M. Smith): The cold seal converter task has been divided into three phases. Phase one involves the construction of a heat pipe-like device to investigate the operational characteristics and stability of cesium-inert gas interfaces. In the second phase, an emitter assembly will be inserted into the heat pipe to demonstrate that polymer O-rings can be used to power producing thermionic devices. Phase three will further investigate the interactions of the inert gas-cesium interface with the cesium above the inert gas.

The design of the heat pipe and test stand was completed during this reporting period. Fig. 1 shows the heat pipe, collector and associated hardware. The gas handling system was also designed and partially fabricated. A schematic of the gas handling system is shown in Fig. 2. Several design considerations of particular concern were evaluated, resulting in some changes from the original design previously reported.

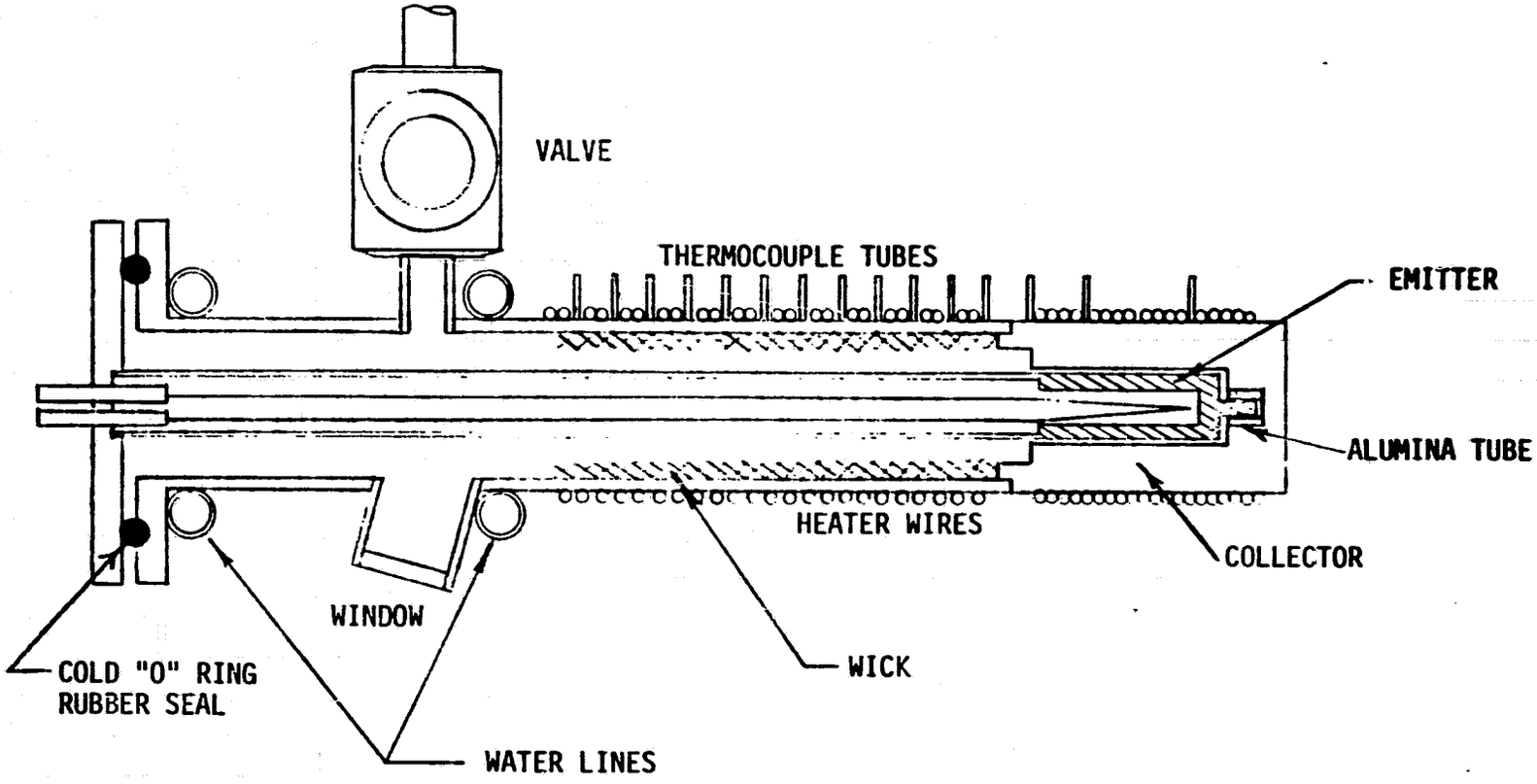

Fig. 1 Cold-Seal Converter Design

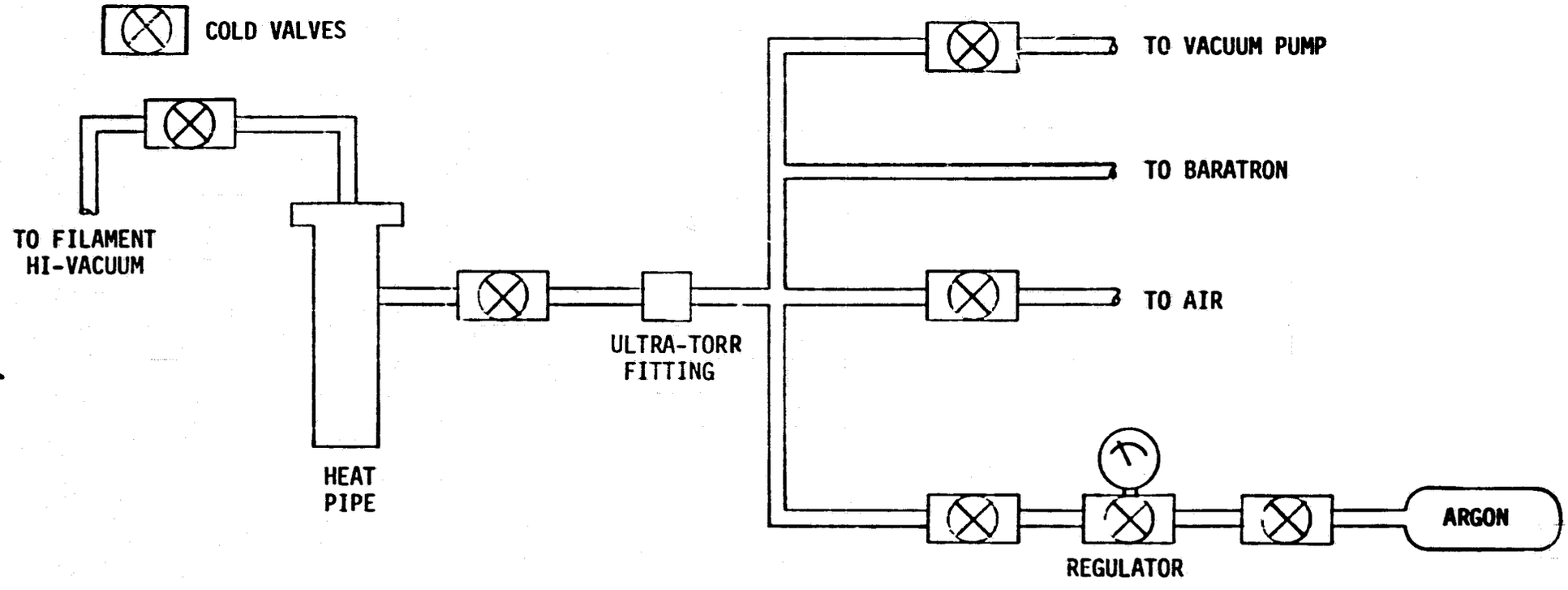

Fig. 2 Cold-Seal Converter Gas System

A. Cesium Control: most previous experiments involving cesium/inert gas interfaces were operated using horizontal tubes and separate cesium reservoirs. It was determined that in this device the cesium pressure would not be a direct function of reservoir temperature but was more influenced by the argon pressure and the wall heat flux. In this design the heat pipe wick acts as the reservoir with the height of the cesium/argon interface controlling the volume of cesium vapor.

B. Heat Pipe Rotation: the original design used a fixed frame with a pivoting heat pipe. That design required that 24 thermocouples, 2 water cooling units, and 6 heater leads be twisted 180 degrees. This was found to be cumbersome and unnecessary. The present design uses a light cubical frame with a fixed heat pipe. The frame will be rotated to simulate inverted thermionic converter operation.

C. Heater Brazes: the original design called for the heater wire to be copper brazed onto the stainless steel heat pipe. This was a potential problem since the copper braze could oxidize at the operating temperature (600-700°C) in air. Samples were made with several pieces of S.S. tubing with heater wires brazed on them. These were heated for one hour at the operating temperatures. The copper braze showed some oxidation and spalling but withstood numerous thermal cyclings.

D. Stainless Steel Decomposition: during the heater braze test the S.S. tubing experienced severe oxidation and spalling. The surface came off in large black flakes. It is believed that this was caused by hydrogen embrittlement of the S.S. during brazing in a hydrogen furnace. This was substantiated when tests were run at the operating temperature in air after outgassing the stainless steel in vacuum.

E. During the heater test a suitable means for easily attaching a durable connector to the fine nichrome heater wire was devised.

F. A major design consideration was ensuring the proper spacing between the emitter and collector. This will be accomplished as shown in Fig. 1 by including an alumina centering tube in the collector. The inside of the alumina will be made concentric with the collector wall to within 0.0005 inches.

Fabrication of the heat pipe/collector section and the gas handling system will be completed during the next reporting period. Also, it is expected that the cesium-inert gas interface tests will be completed in August and the converter will be operated in September.

Distributed Lead (L. L. Begg, B. Carlsmith): A modification of the distributed lead concept which uses blade-type current leads in place of stud-type leads was devised during this period. The standard converter single lead design, the stud-type distributed lead, and the new blade-type lead are shown in Figs. 3, 4, and 5. The primary disadvantage of the single-lead design is the need for a thick and expensive emitter electrode in high-current converters in order to minimize resistive power losses. The distributed lead eliminates this problem by periodically removing current from the emitter and delivering it to a low-cost emitter current bus. The stud-type distributed lead is the most straight-forward way to accomplish this goal, but it is relatively complex and poorly suited to accommodating large amounts of differential thermal expansion between the emitter and collector. Magnetic field effects near each post can also be troublesome. The blade-type lead reduces the complexity of the design while permitting differential thermal expansion parallel to the blades. In addition it facilitates fabrication of a converter since a collector segment between blades can, in principle, be removed without removing the emitter current leads and emitter bus.

Several tests were run to determine the fabrication feasiblity of the stud-type distributed lead desig.. One problem is attaching the flexible portion of the distributed lead to the emitter. Since there would be hundreds of these joints in a THX cell, it is important that

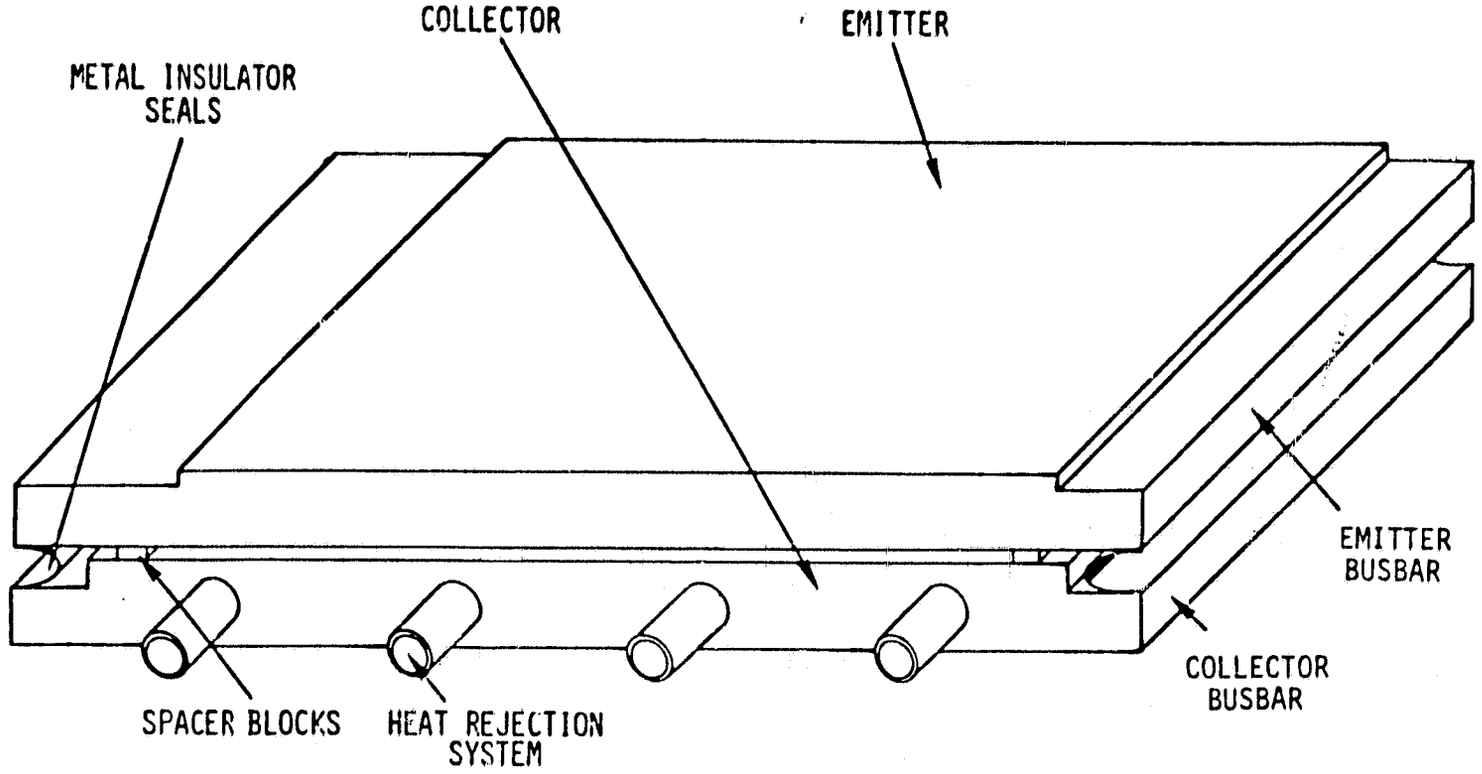

Fig. 3 Conventional Single Emitter Current Lead Design

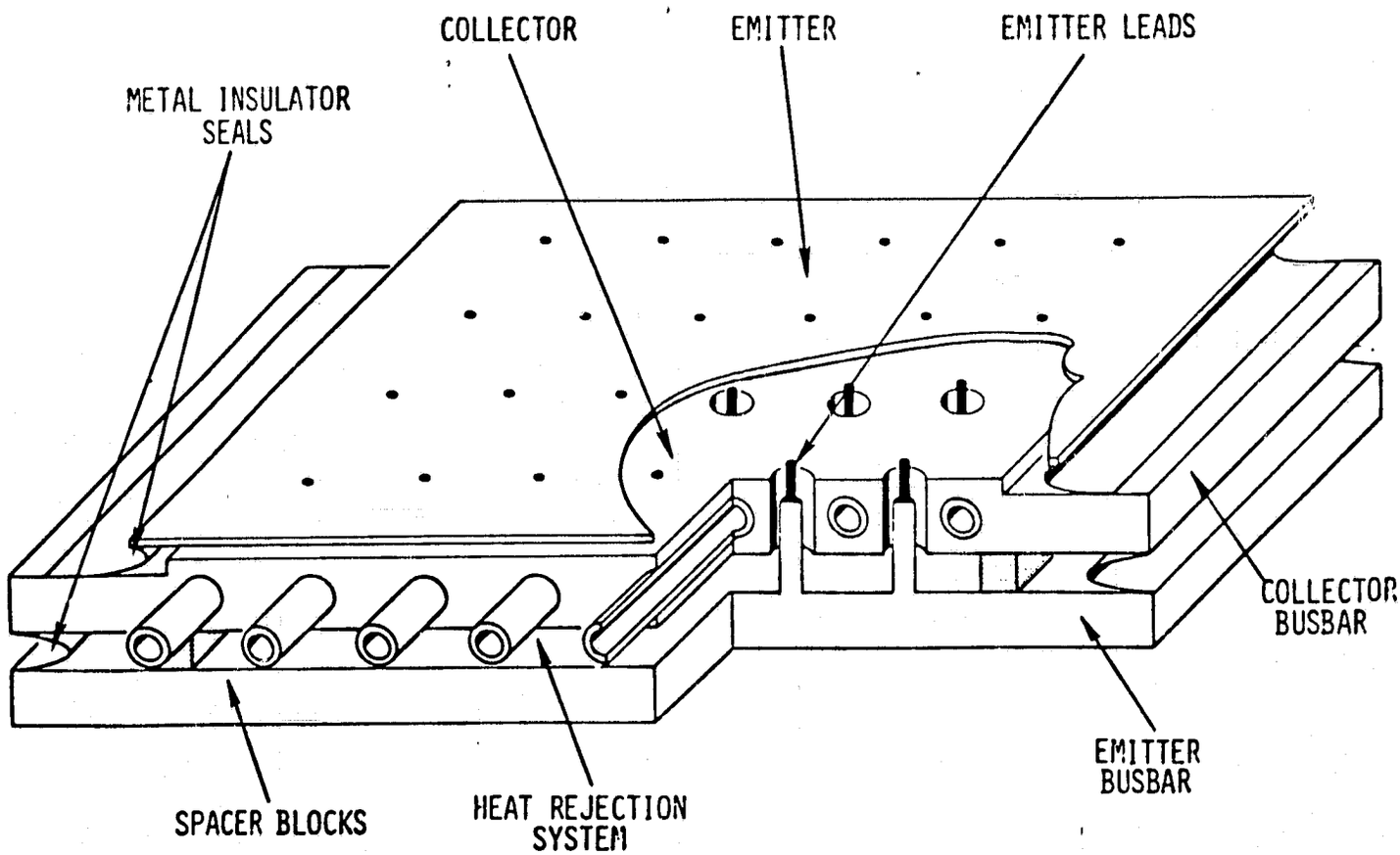

Fig. 4 Stud-Type Distributed Emitter Current Lead Design

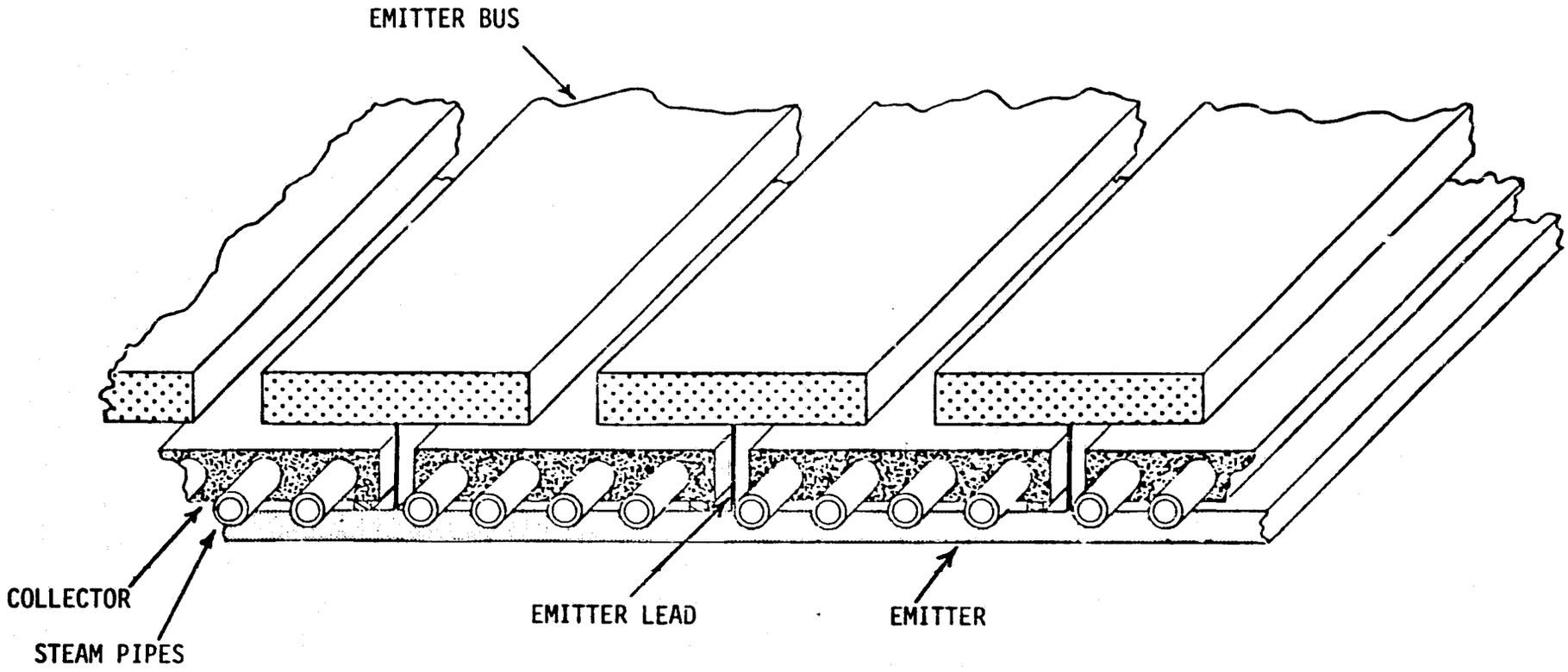

Fig. 5 New Blade-Type Distributed Lead Design

the joint be reliable and reproducible. An unsuccessful attempt was made to TIG weld thin nickel wire to a large mass of nickel. An alternative technique using spark welding was developed and reproducible, high-quality welds were obtained.

High Current Converters: An HC-2 design using a segmented collector and the new blade-type distributed lead is being investigated. This approach looks very attractive and supporting design calculations will continue in July. The design minimizes the problems associated with close electrode spacing, bellows closure, collector cooling and numerous distributed lead attachment joints.

Steam will be used to cool HC-2, instead of jet impingement of room air. While not yet specified, a smaller diameter (~8") than that used in ZEPO is likely as a result of recent system calculations.

Disassembly and examination of ZEPO was begun in order to provide as much design information for HC-2 as possible.

1.1.2 Heat Transfer Technology (L. L. Begg, D. Johnson)

Introduction: The objective of this task is to provide the heat transfer technology needed to couple the THX power module to the heat source, including the basic heat pipe and methods of protecting it from the heat source. Previous development of high temperature heat pipes has established the basic technology, as demonstrated in Mo/Li heat pipe life tests exceeding 15,000 hours at 1700°K.[3] The more critical task is development of protective hot shells capable of long life times in a combustion environment. Complementary work on the development of protective hot shells by Thermo Electron Corporation has concentrated on ceramic (SiC) protective hot shells on refractory metal substrates and free standing superalloy emitters. This task will develop combustion protection techniques based on the use of refractory metals for strength, with protection provided either by superalloy cladding or self-healing coatings which exist in equilibrium with the combustion environment. The latter technique, the maintenance of a protective hot shell in equilibrium with the combustion

environment, is one of the most attractive approaches to ensuring a reliable hot shell. The isothermal-stationary nature of the THX heat pipe makes it particularly adaptable to this form of protection.

During this contract period a furnace will be built to permit the addition of additives to provide simulated slag, silica, and other desired coatings. The furnace will then be used with suitable test specimens in order to determine the stability of each hot shell over a period of time.

Current Effort: Work on this task was initiated during this period, beginning with a general review of previous efforts to protect refactory surfaces in combustion environments.

A fair amount of development work in the area of metallic coatings was performed during the 1960's. The most promising seemed to be a duplex coating of nickel over chromium on a molybdenum substrate. This system had two primary limitations, oxidation of the nickel overlay above ~2200°F and a thermal expansion mismatch between nickel and chromium which sometimes led to spalling. Advances in nickel alloys and application processes have renewed interest in this scheme. By applying the oxidation-resistant Inconel 671 alloy by explosion bonding to the chromium, a higher operating temperature for this metallic coating system may be attained. The Inconel 671 alloy is more oxidation resistant than nickel used in earlier work. The explosion bonding process produces a near-metallurgical joint. Metals with large differences in thermal expansion have been joined together by explosion welding and successfully thermal cycled without separation.

Four possible sources of explosion bonding were located: the University of Denver, Los Alamos Scientific Laboratory, North West Technical Industries, and Du Pont. Following a trip to the University of Denver and technical discussions with Dr. Jim Mote the University was selected to perform trial bonds between low carbon arc-cast molybdenum and Inconel 671.

The review of silicide coating technology resulted, as expected, in the conclusion that preapplied silicide coatings can be expected to last for only a few hundred hours at 2300°F-2400°F. The effort to provide protection with such surfaces will thus concentrate on establishing a vapor pressure of silica or other materials in the combustion atmosphere which can serve to repair or replace flaws in the coating as they occur.

Bill Martini, a heat transfer and materials specialist, was consulted to provide additional ideas for providing molybdenum oxidation protection. His suggections included surrounding the heat pipe with a close-fitting cylinder of SiC. By filling the space between the SiC and the heat pipe with hydrogen, adequate heat can be transferred across the annular gap without an excessive temprature drop. By keeping the hydrogen under slight pressure, joints in the SiC cylinder and any defects which may form in the SiC will merely leak hydrogen out, preventing combustion gases from leaking inward.

Since hydrogen, under slight pressure, will exist in the gap between the heat pipe and SiC, it is important that there be a low permeability for hydrogen through the SiC. A permeability test made of Norton "Crystar" SiC showed an unacceptable volume of hydrogen would flow through a wall made of that material. Fig. 6 shows the results of the test. "KT" SiC, manufactured by Carborundum, is sufficiently dense and will be used to test the concept.

Bids for fabricating a small life-test furnace were received from W. P. Keith Co., Harper Furnaces and Kilns, Harrop Precision Furnace and Bolt Technical Ceramics. All of the furnaces have a working volume of 12"x12"x12" and will operate up to 3000°F. Since all of the bids received were higher than permitted by the budget the furnace will be built in-house.

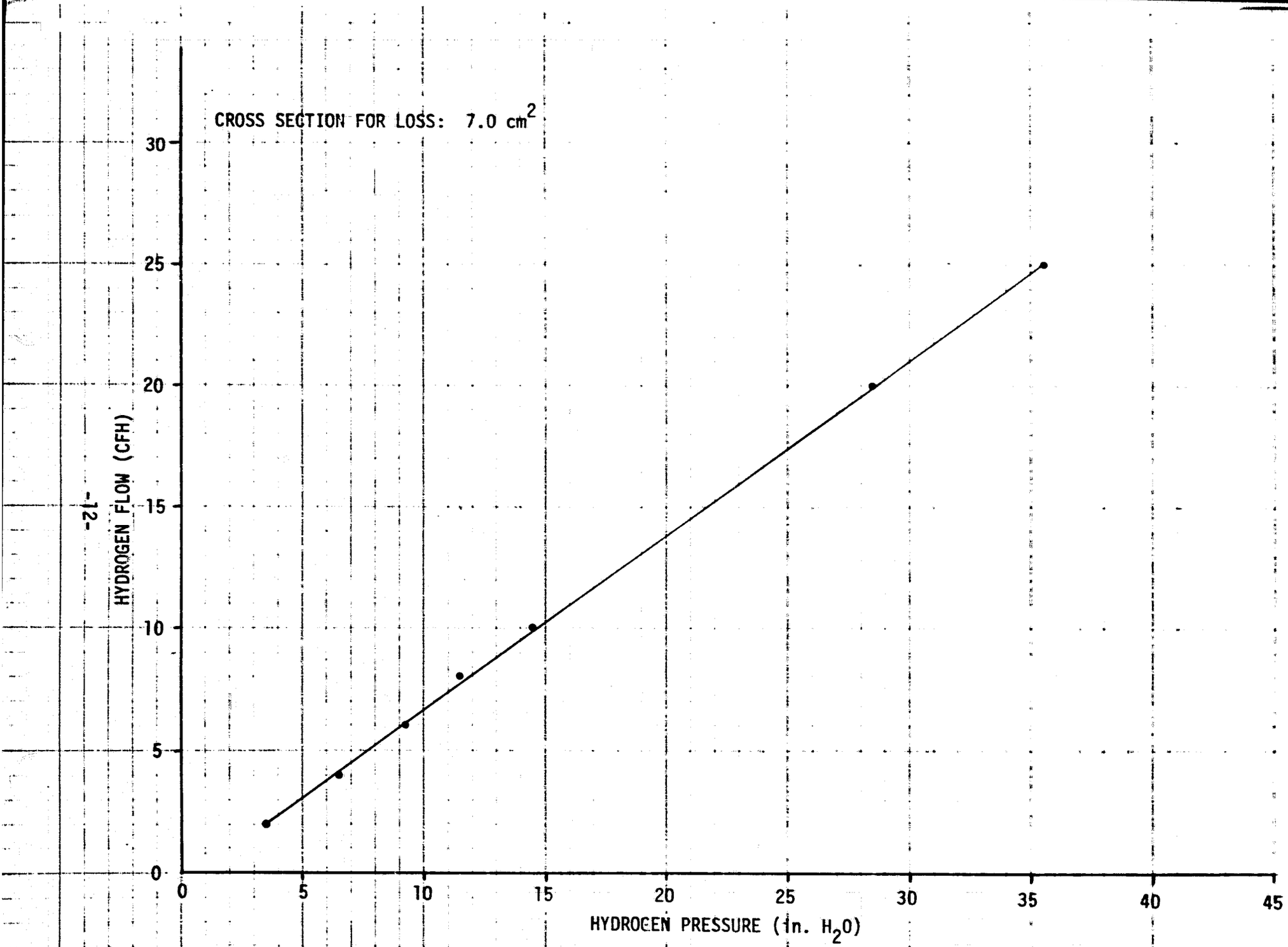

Fig. 6 Hydrogen Permiation through Norton "Crystar" Silicon Carbide

1.1.3 System Analysis (G. O. Fitzpatrick, E. J. Britt)

Introduction: There are a variety of applications for which Thermionic Power Modules could provide significant energy and cost savings. These include utility central station power plants, industrial cogeneration systems, systems incorporating advanced combustors (fluidized bed combustors, gasifiers, etc.), and solar thermal power plants. Each application has special requirements for the converters used in the system. For example, central station power applications require low cost converters with high efficiencies. Low operating and maintenance costs are particularly important in industrial applications.

This task reviews system designs for the most attractive of these applications to determine the probable thermionic operating conditions needed to minimize system electricity costs and maximize energy conservation. The results are then used to guide the converter research and development effort. It has been shown that the use of THX thermionic power modules used as a topping system for coal-fired central station power plants could improve plant efficiencies from their present level, near 33%, to 50%. Such an improvement for all U.S. coal fired power plants could save the equivalent of 10 million barrels of oil daily by the year 2000. The preliminary studies indicate that such THX-thermionic power plants would have capital costs comparable to conventional steam power plants, thus providing electricity at reduced costs while saving energy (up to 25%) and reducing pollution (25-40%).[4,5] Repowering or retrofitting existing power plants with thermionic topping systems could substantially increase their capacity (50% or more) with no more requirement for cooling water. Based on these preliminary results a more detailed system study has been initiated, Task 2.2 in this program.

During this contract period a preliminary study of the cogeneration application will be performed as part of this task. The single point designs used in the independently funded "Cogeneration Technology Alternative Study" will be reviewed and the most attractive industrial application selected for optimization in order to more accurately project energy savings and system costs.

Current Effort: Since the "Cogeneration Technology Alternative Study" has not yet been completed no work was accomplished on this task during this period.

1.2.1 Converter Technology (M. L. Manda)

Introduction: The objective of this task is to increase basic converter performance using improved converter designs, materials, and processing techniques suitable for subsequent incorporation into practical prototype power modules. The effort concentrates both on improved efficiency and power density and on reducing the emitter temperature needed for high performance. Reduced emitter temperatures in turn improve compatibility with the heat source and extend operating life.

Basic converter performance can be roughly characterized by a quantity called the "barrier index" V_B. This index is a measure of the voltage loss within a given converter compared to an "perfect" converter operating at the same emitter temperature. The barrier index for such a "perfect" converter is V_B = 0 eV. Useful estimates of both converter efficiency and output power density can be projected once the barrier index of a device is specified. Fig. 7 shows such efficiency projections and output power projections are shown in Fig. 8.

The best converter output power performance obtained to date in the U.S. thermionic program is characterized by a barrier index V_B ~1.9 eV. This result has been obtained both by LaB_6/LaB_6 electrodes[6] and W_{110}/WO_x electrodes.[7] The workers in the USSR claim barrier indices as low as V_B ~1.7 eV, results not yet verified in the U.S.[8]

While output power densities can be measured in any converter actual operating efficiencies can best be accurately measured in cylindrical converters. For comparison Figs. 9 and 10 show the measured electrode efficiency and average operating electrode power densities of the cylindrical converters tested at Gulf General Atomic between 1965 and 1973.[9] The operating range for the four NASA/JPL cylindrical converters described in the previous report[10] are shown for comparison in botn plots. The output power of the planar W/WO_x converter with V_B ~1.9 eV is also shown for comparison.[7] As

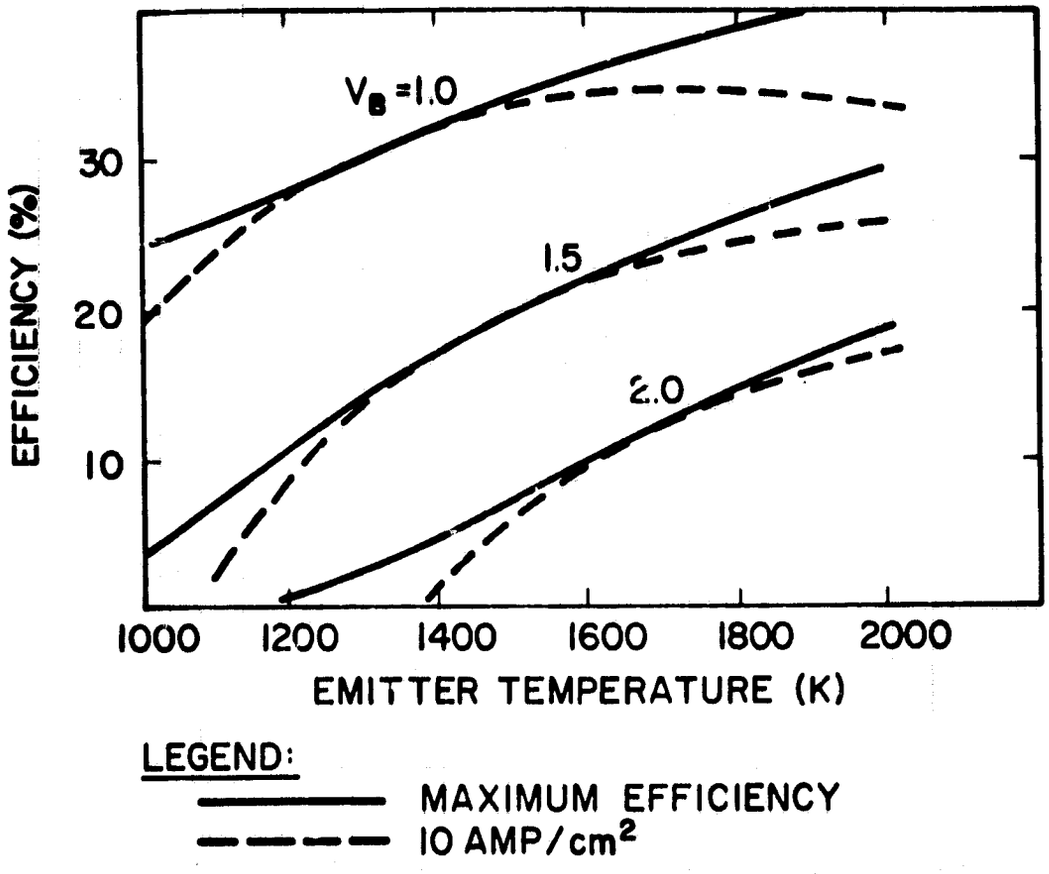

Fig. 7 Projected Converter Efficiency

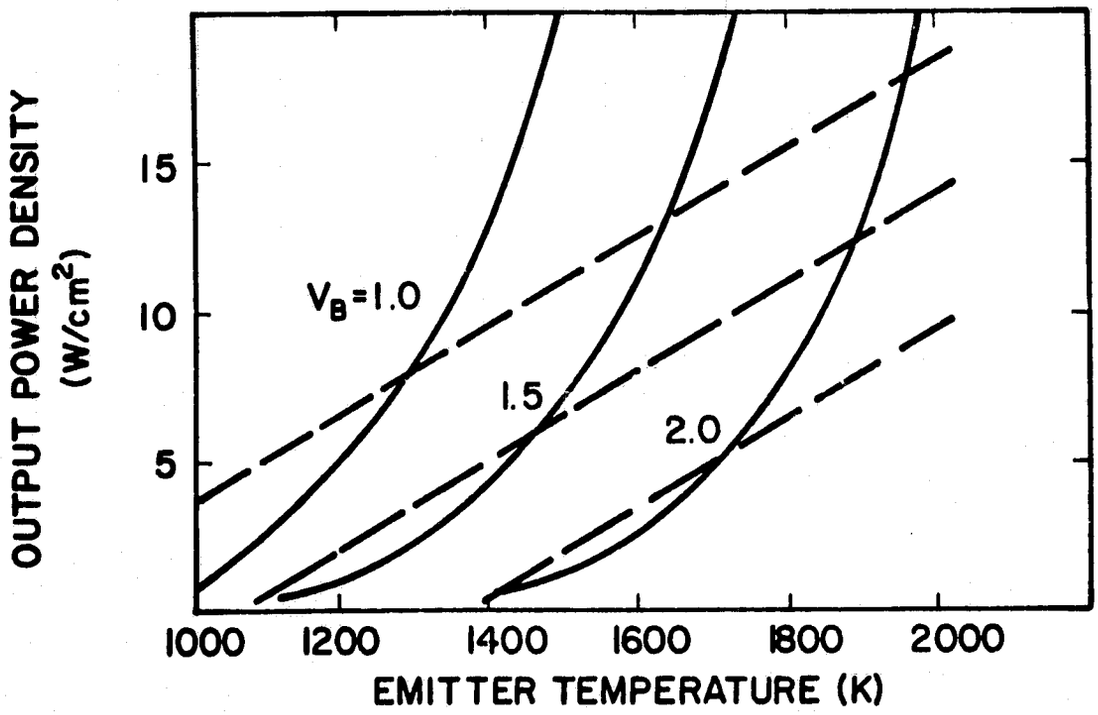

Fig. 8 Projected Converter Output Power Density

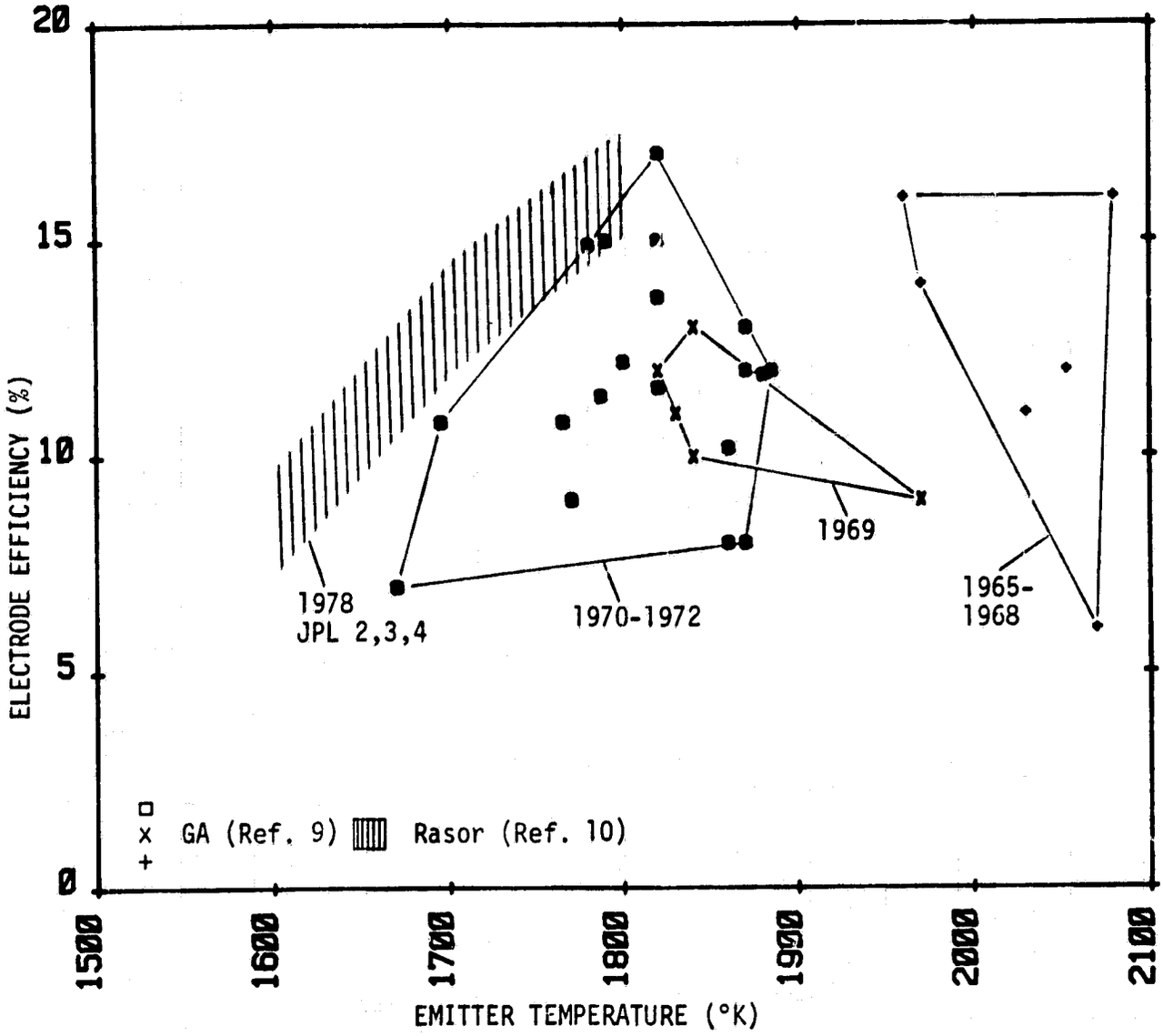

Fig. 9 Cylindrical Converter Efficiency Performance

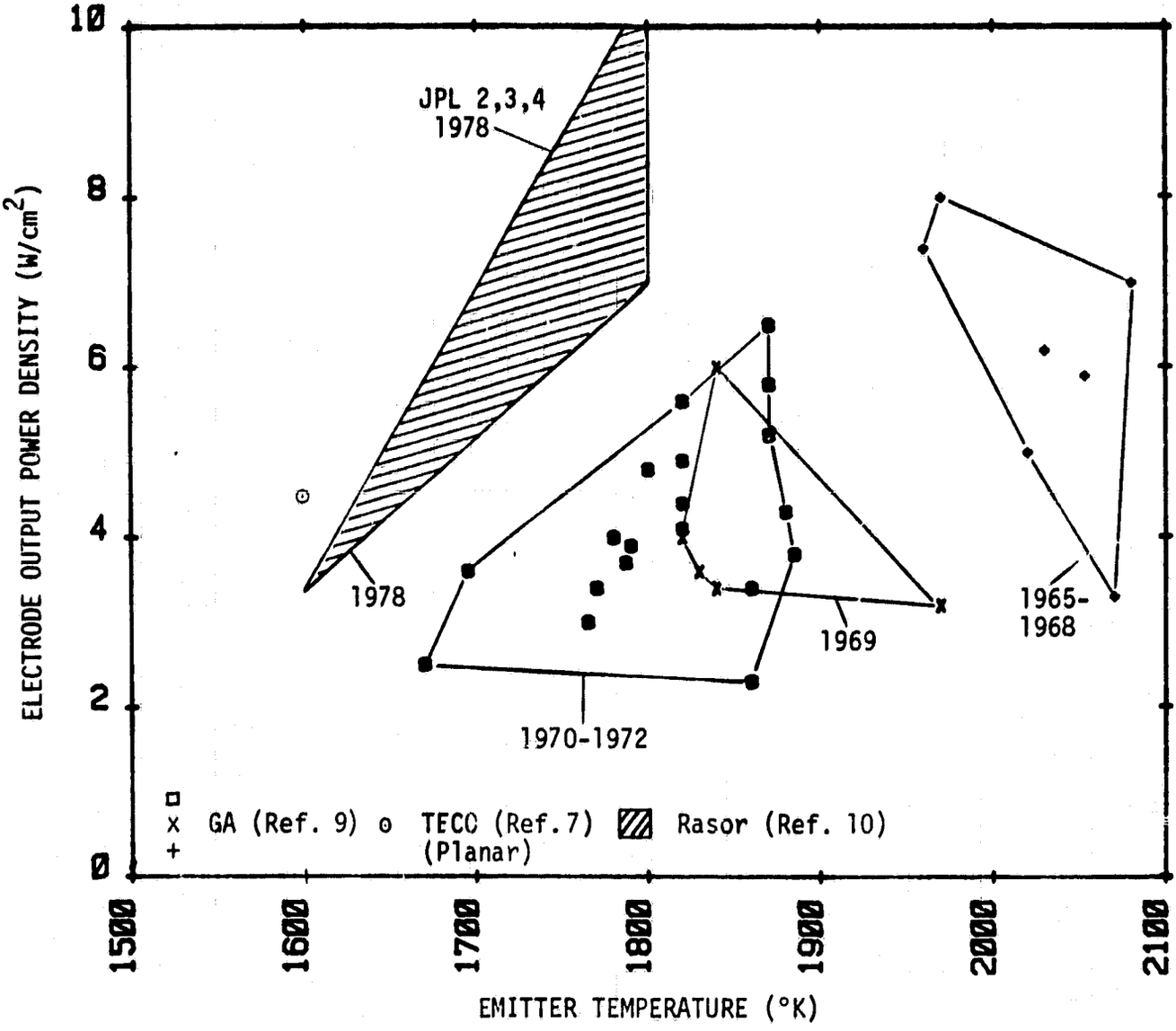

Fig. 10 Cylindrical Converter Output Power Performance

can be seen steady progress is being made on all fronts, reducing V_B, reducing emitter temperatures and improving efficiency and power density.

Both analysis and converter tests show that improvements of 0.1 eV to 0.2 eV are possible using structured electrodes, but no attempt has yet been made to use a combination of structure and low collector work function materials. A number of attractive surfaces which in combination could reduce the effective collector work function, and barrier index by up to 0.5 eV have been identified. Finally, analysis, supported by basic plasma experiments, indicate that barrier index reduction of up to 0.4 eV should also be possible by using more efficient auxiliary ion sources to generate the interelectrode plasma.

To study and evaluate these promising concepts a series of converter tests is being performed using three types of standard test vehicles. Standard variable spacing planar converters (SPC) are used to obtain accurate J-V data, refined cylindrical converters (RCC) are used to obtain energy balance and efficiency data, and an inexpensive standard cylindrical converter (SCC) is used for screening purposes. In addition special converters are designed to meet the specific needs of some advanced concepts.

Current Activity:

Standard Converters (M. Manda): Task activities were defined in detail during the previous reporting period and fabrication of SPC converter body parts was begun in this reporting period. Parts of 10 converters were machined, cleaned, and outgassed. The electrodes for SPC-9 were specified and machined. Both the emitter and collector will be smooth Mo surfaces. This converter is intended to be a standard to which subsequent data on structured electrodes may be compared. Testing of SPC-9 will begin in the next reporting period. SPC-10 will have a structured molybdenum collector. The geometry of the structure for the SPC-10 collector will be specified in the next reporting period.

Converter fabrication has been delayed by a series of equipment problems. The longest delay was caused by a failure of the nitrogen removal apparatus, which is a part of the argon box purification system. This piece of equipment was repaired, and a safety system was installed to prevent future problems. The safety system completely isolates the nitrogen removal system from the argon box recirculation when oxygen levels in the box become too high.

Deficiencies have been found in the ceramic-metal seals which were to be used in the SPC series of converters. These seals were made from Coors AD998 alumina and Nickel 201 metal members directly brazed together using zirconium. Following outgassing at 775°K, almost all of the seals leaked. The failures were attributed to several factors. First, it is likely that the metal member does not have enough compliance. Thus, stress induced fracture may have occurred. Second, the ceramics were not lapped, requiring the use of extra zirconium which contributes to the brittleness of the braze joint. Finally, zirconium can be a grain growth promoter in alumina, and stresses generated at the boundaries of large grains can induce microfractures. The braze region was examined optically at 140x magnification, and this grain growth was confirmed near the zirconium. Examination of the ceramic-metal seals is continuing. Other suppliers and configurations are being evaluated.

A complete second set of converter test stand mounting hardware was fabricated. These parts will increase the exchange efficiency of the converters within the SPC test stand.

Modifications of the SPC to accommodate special surfaces are being considered. It appears that the Zr-O-W and W-O-Cs electrodes will require special handling to permit their incorporation into a converter.

Current Acitivity:

Bloss Tube Experiment (N. Rasor): The highest performing converter ever reported was a plasmatron device built by W. Bloss in the early 1960's. This converter apparently operated with third generation performance, although its power density was low (~1 W/cm^2), and its geometry is apparently impractical. This task has the objective of reproducing the Bloss results with an essentially identical converter (i.e. Ba dispenser emitter, Cs-Ag-O collector, large radial current divergence, inert gas plasmatron operation with garrote ionizer). The tests should either confirm or refute the exceptionally favorable data reported by Bloss. If his results are confirmed the origin and nature of the uniquely beneficial processes at work will be established using modern diagnostic and analytical techniques. Based on this insight methods for applying these processes to practical converters will be sought.

A device was constructed (Fig. 11a) which faithfully reproduced the original Bloss tube design[11] (per available knowledge, e.g. Fig 11b) with the following exceptions, which were thought to be minor:

a. The cesium vapor inlet was in the end region of the tube instead of through the collector (between the micas).

b. The cesium source was a glass ampoule of liquid cesium instead of a Si-Cs_2CrO_4 mixture.

The tube was processed identically, within available knowledge, as prescribed by Bloss. However, when the cesium ampoule tip was broken, the glass enclosure of the magnetic striker also broke, releasing an air-burst into the tube after the prescribed bakeout and collector oxidation steps. It was decided to continue at least as a procedure-familiarization run.

After the air-burst was pumped out, the prescribed cesiation of the collector was performed, and the "forming" process was observed to follow the qualitative behavior described by Bloss[11] and Weber[12] i.e. the successive color changes, and the rapid increase and eventual broad maximum of photo and thermionic emission from the collector). The minimum work function inferred from the thermionic emission was in the vicinity of 1.2 eV at 160°C.

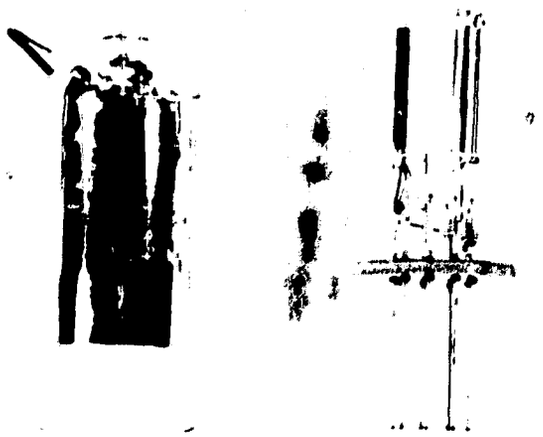

Fig. 11a Reproduction of Bloss Plasmatron Tube

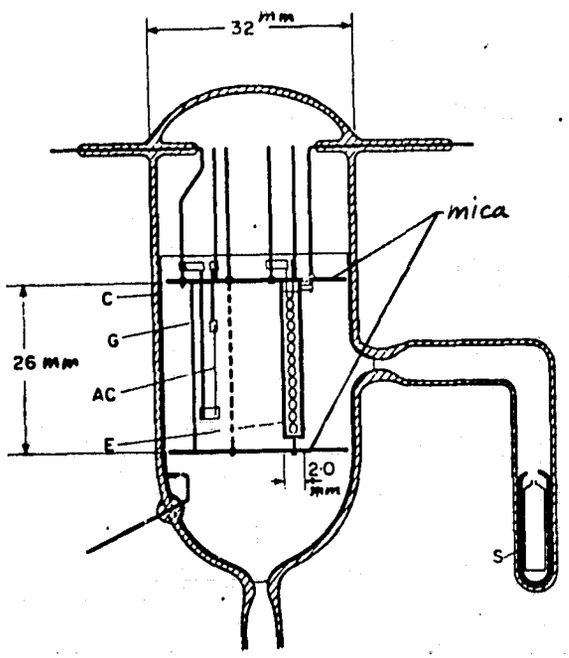

Fig. 11b Original Bloss Tube Design:

A = collector (oxidized and cesiated silver layer on inner surface of envelope); G = nickel garrote; K_1 = auxiliary emitter (oxide-coated 1-1/2 mil dia W wire); K_2 = main emitter (oxide-impregnated sintered nickel cylinder with interval heater); C = cesium source (Si + Cs_2CrO_4).

The tube was filled with Krypton at 200 microns pressure, and operated as a plasmatron. The qualitative behavior was as expected, but both emitters appeared to be poisoned. The auxiliary emitter burned out shortly after being raised to a sufficiently high temperature to approach the required auxiliary current. Presumably the poisoning arose from residual air due to the air-burst.

The tube envelope was opened, and the fragile Bloss-type auxiliary emitter was replaced by a more rugged indirectly-heated commercial oxide emitter. This should not affect the electrical characteristics of the device since the emission from this emitter presumably is space-charge limited. Somewhat more auxiliary heater power will be required, however. If this is important, the Bloss-type emitter can be restored after familiarity is gained with operation of the device.

The tube was resealed and the processing repeated. Gas evolution observed at 120°C and 180°C during this bakeout presumably was due to decomposition of Cs_2O and Ag_2O as the collector surface was reduced to silver. Weber states that repeated oxidation and reduction are beneficial to the Cs-Ag-O surface. During the reoxidation, however, the lower half of the collector was badly eroded, indicating that it was not sufficiently thick, at least for repeated oxidation. Also, the cesium ampoule striker enclosure again broke, again releasing an air burst into the tube. Again processing and operation were continued mainly for familiarization since comparison with the Bloss data would be highly questionable.

Forming proceeded identically as before in qualitative accord with the Bloss and Weber description. The collector work function inferred from thermionic emission was nearly constant at about 1.2 eV over the temperature interval 350-443°K. This is somewhat higher than the 1.0-1.1 eV reported by Bloss at 300°K and by Weber at 350-443°K. More care was taken this time to thoroughly activate and outgas the emitter in vacuum to minimize any residual contamination from the air-burst. During such initial emitter operation the collector work function would gradually rise about 0.1 eV, but could be restored by recesiation.

Plasmatron operation at 200 micron Kr pressure was stable and for the most part qualitatively in accord with the Bloss data and with experience from other plasmatron devices. Several important differences from the Bloss data were observed, however:

1. The minimum barrier index (based on collector area) was in the vicinity of 1.6 eV (compared with the <1.3 reported by Bloss).
2. The saturation current of the main emitter seemed to be <200 ma (compared to the >1.3 amp reported by Bloss), although this could have been due to the garrote limitation described in 3 below.
3. The auxiliary current showed two modes of operation: an efficient mode below 3 ma with the visible discharge only outside the garrote, and a less efficient mode above 3 ma with the discharge only inside the garrote (Bloss used a 5 ma current).

A completely new tube is being constructed which will eliminate the cesium ampoule (a Cs_2CnO_4 source will be used a la Bloss), will have a much thicker silver collector, and will have a finer grid on the garrote to prevent penetration by the discharge. In the mean time, the existing tube will be operated for further familiarization with the gross device operating characteristics.

In summary, many of the desirable qualitative characteristics of the Bloss device have been observed. The quantitative deficiencies observed may be due to component design and processing deficiencies encountered which should be corrected in the new tube under construction.

1.3.1 Converter Performance Analysis (E. J. Britt, J. McVey)

Introduction: The objective of this task is to develop analytical models of converter characteristics to guide converter development and provide diagnostic tools. Previous efforts in this program have resulted in models which describe the characteristics of diodes operating in the ignited and the unignited modes, and of converters using auxiliary ion sources. These models have been used to identify and better understand the most important physical phenomenon occurring in the converter and

their impact on converter performance. The models are continually refined to explore new possibilities for converter improvement. Emphasis during this contract period will be on possibly beneficial two-dimensional effects, such as those found in structured electrode devices or those which may have existed in the very high performance Bloss plasmatron converter. Other possibly beneficial phenomenon, such as thermoelectric effects, will be studied.

Current Effort: The converter analysis effort during this period has concentrated on two areas: calculation of the electric fields in the plasma of a converter, including thermoelectric and divergence effects, and refinement of the auxiliary ion source converter performance program.

The electric field of the thermionic converter was investigated as a possible explanation for the anomalously good results obtained by Bloss's experiment. The calculations were carried out in conjunction with Dr. Maria Stoenescu of Princeton University during her visit to our facility in June. In order to do this calculation, the transport coefficients calculated by Stoenescu and Heinicke,[13] for the ignited mode conditions were used. Other calculations were made of the electric field with the electron neutral scattering removed in hopes of simulating a favorable condition for the electric field in the converter.

The calculation showed that the thermoelectric effect should have a very small contribution to the electric field in a thermionic converter for normal ignited mode conditions. This is not a surprising result, considering the nature of the electron neutral scattering cross section for cesium. However an unexpected result of the calculation is that the ion temperature gradient across the interelectrode space produces an ion thermoelectric effect which is of a similar magnitude and opposite sign to the electron thermoelectric effect and thus tends to cancel any thermoelectric effect. This is illustrated by Eq. (1)

$$\vec{E} = \underbrace{-\frac{1}{n\,\mu_e}\frac{T_i}{T_e + T_i}\vec{\Gamma}_e}_{\text{Electron Ohmic Term}} + \underbrace{\frac{1}{n\,\mu_i}\frac{T_e}{T_e + T_i}\vec{\Gamma}_i}_{\text{Ion Ohmic Term}}$$

$$+ \underbrace{\frac{T_e}{T_e + T_i}\left(k_i^T + 1\right)\frac{k}{e}\nabla T_i}_{\text{Ion Thermoelectric Term}} - \underbrace{\frac{T_i}{T_e + T_i}\left(k_e^T + 1\right)\frac{k}{e}\nabla T_e}_{\text{Electron Thermoelectric Term}}$$

$$- \underbrace{\frac{1}{en}\frac{T_e}{T_e + T_i}\vec{R}_{ie}}_{\text{Ion Drag Term}} \qquad (1)$$

The ion thermoelectric term is weighted by the ratio of the electron temperature to the sum of the electron and ion temperatures while the electron term is weighted by the ratio of the ion temperature to the sum of the electron and ion temperatures. The ion temperature in normal converter plasmas are usually substantially less than and never larger than the electron temperature. Furthermore, the ion temperature gradients for both ion and electron slopes in the same direction and are approximately the same magnitude. Thus, the ion term tends to be as least as large of greater than the electron term in nearly all cases.

Numerical calculations of the thermoelectric effects for a typical ignited mode case are shown in Figs. 12, 13, and 14. The plots in these figures show only a small contribution to the thermoelectric effect from temperature gradients, even when the electron neutral scattering is removed and only plasma scattering is retained.

Another interesting pieces of insight that came from the electric field calculation is that the divergence of the plasma causes a contribution to the electric fields which should be beneficial to converter operation. Since the Bloss experiment contains a small diameter emitter

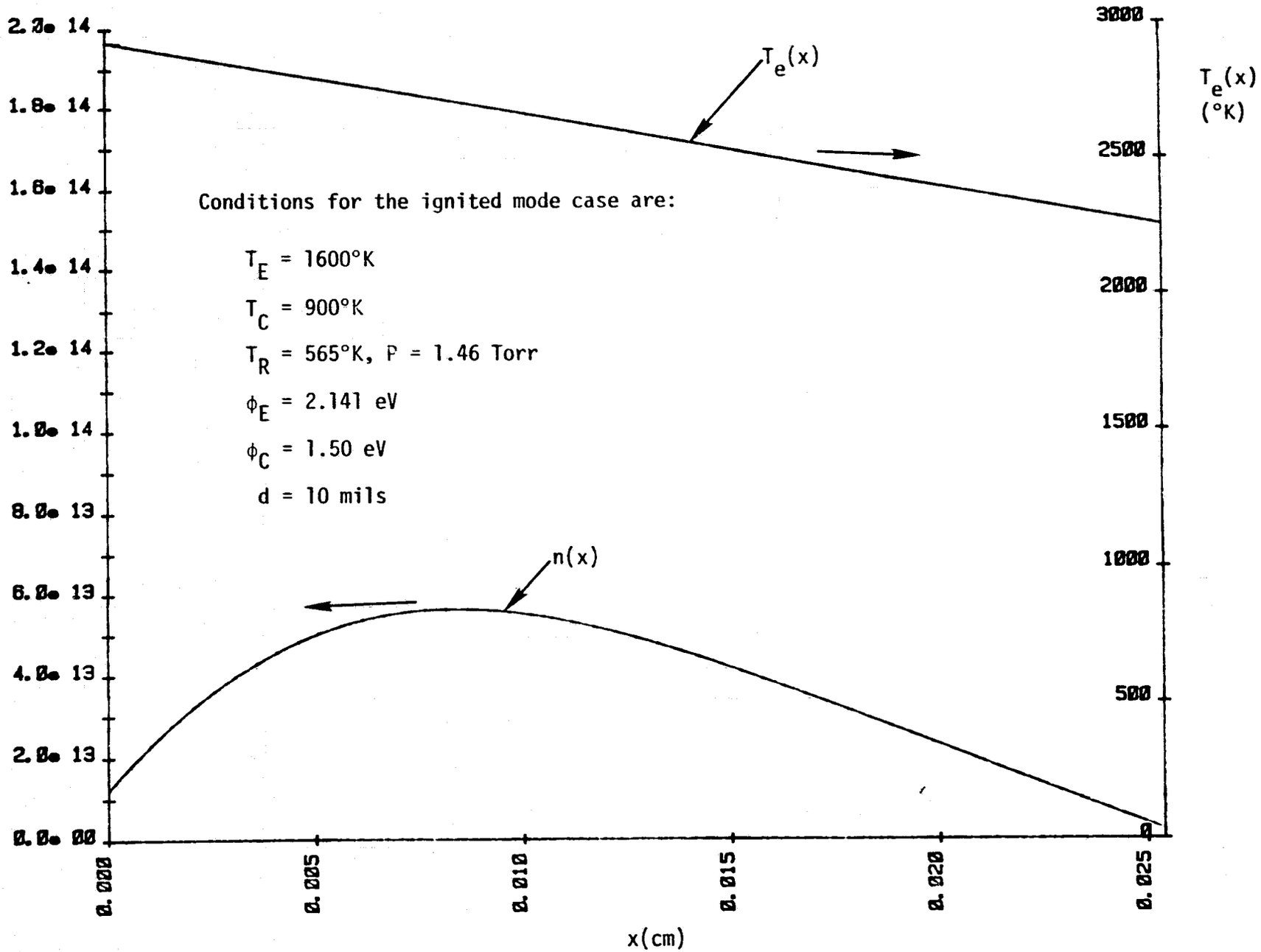

Fig. 12 Calculated n(x) and T_e(x) for the Typical Ignited Mode Case

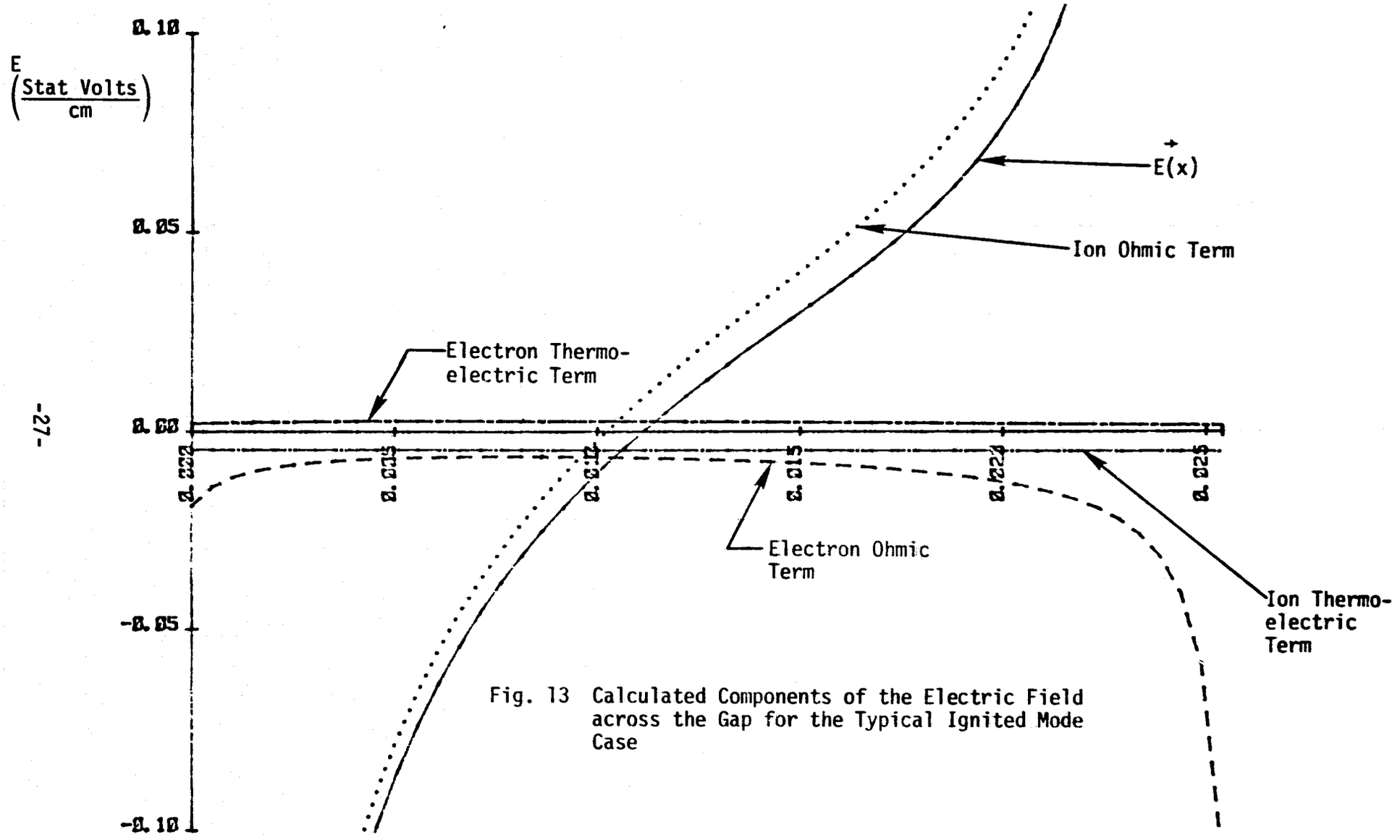

Fig. 13 Calculated Components of the Electric Field across the Gap for the Typical Ignited Mode Case

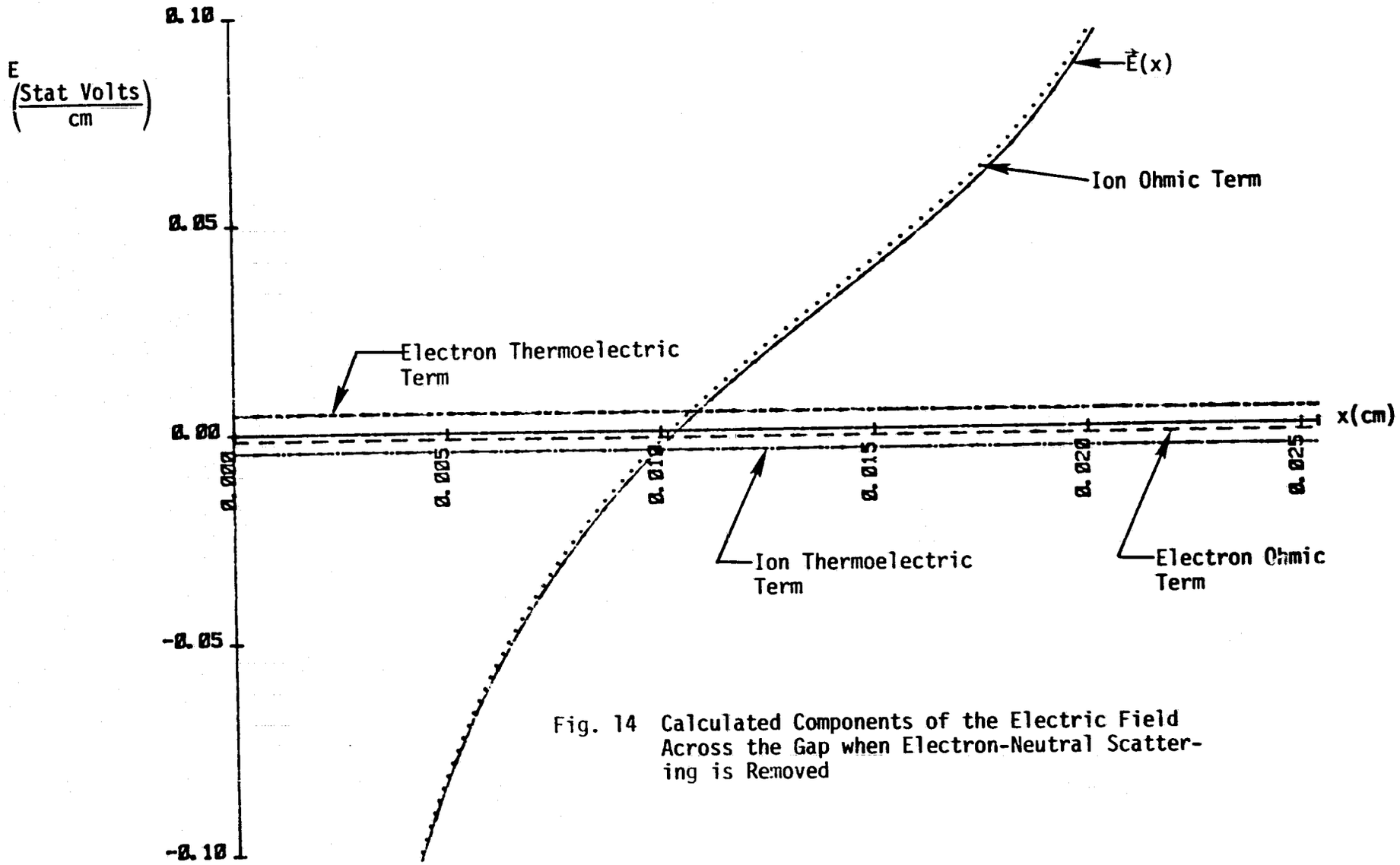

Fig. 14 Calculated Components of the Electric Field Across the Gap when Electron-Neutral Scattering is Removed

located in a large diameter cylindrical collector there was a substantial divergence of the plasma in that case. It's postulated that divergence effects may have been responsible for the improvement in performance which he observed. Future work will examine this promising possibility in more detail.

A number of improvements were added to the AIS (Auxiliary Ion Source) model. First, the scattering cross sections for cesium gas were added to the model in order to allow the examination of the cesium unignited mode. The effects of area ratios and variation of the collision cross section with electron temperature were also included. Recombination was included in the model but as reported previously this produces only a very small effect which is negligible in most cases of interest. The calculation of the electron temperature and the plasma voltage drop were also improved. The equations in the computer algorithm used in the current AIS model are given in Appendix A of this report. Fig. 15 shows a flow chart for the current AIS model.

During a previous effort, a set of J-V curves calculated by the auxiliary ion source model showed very attractive performance for a xenon plasmatron which had a high emitter saturation current. These J-V curves were published in a previous bimonthly report (November-December 1978). The performance predicted by the updated AIS model for a xenon plasmatron with the high saturation current of 154 A/cm^2 was recalculated. The results are shown in Fig. 16. The updated model gives a performance envelope for this case, which has a ~.1 to .2 volts larger barrier index. In Fig. 17 a similar family of J-V curves is shown for a new saturation current of 36.1 A/cm^2. The reduction of the saturation current does not substantially harm the performance of the converter at or below 10 A/cm^2 as can be seen by comparing Fig. 17 and Fig. 16. Even lowering the saturation current to as low as 8.5 A/cm^2 provides attractive performance for current densities in the vicinity of 4 to 5 A/cm^2, as can be seen in Fig. 18. A case was also calculated for the 36 A/cm^2 saturation current with the pressure of 1 Torr instead of 10 Torr. The pressure reduction results in increased performance as shown in Fig. 19. In Fig. 20, a set of J-V curves at the 1 Torr pressures was calculated with the emitter work function as the parameter for the family. Inspection of Fig. 20 shows

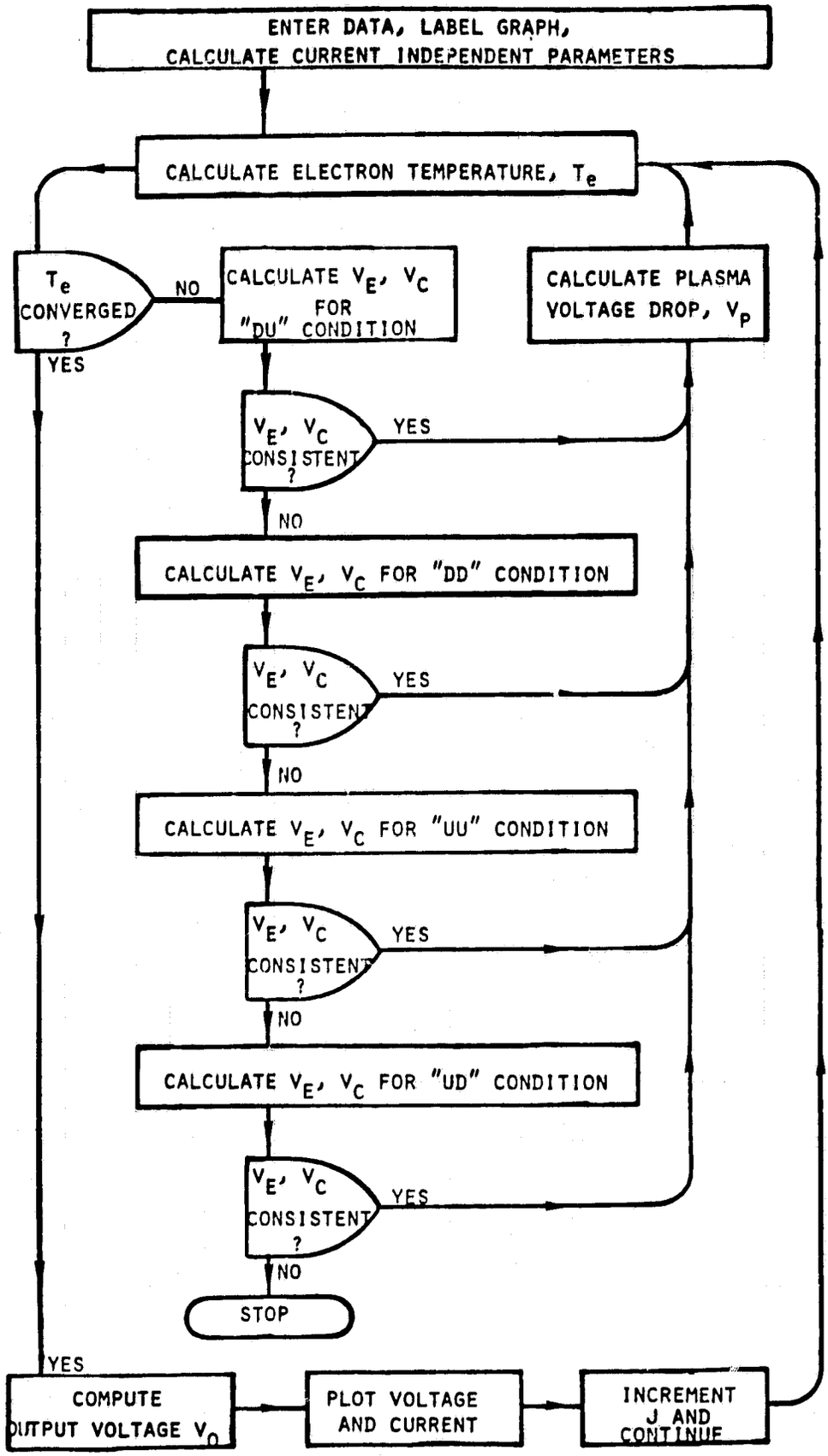

Fig. 15 Program Flow Chart

6/22/79 XENON PLASMATRON

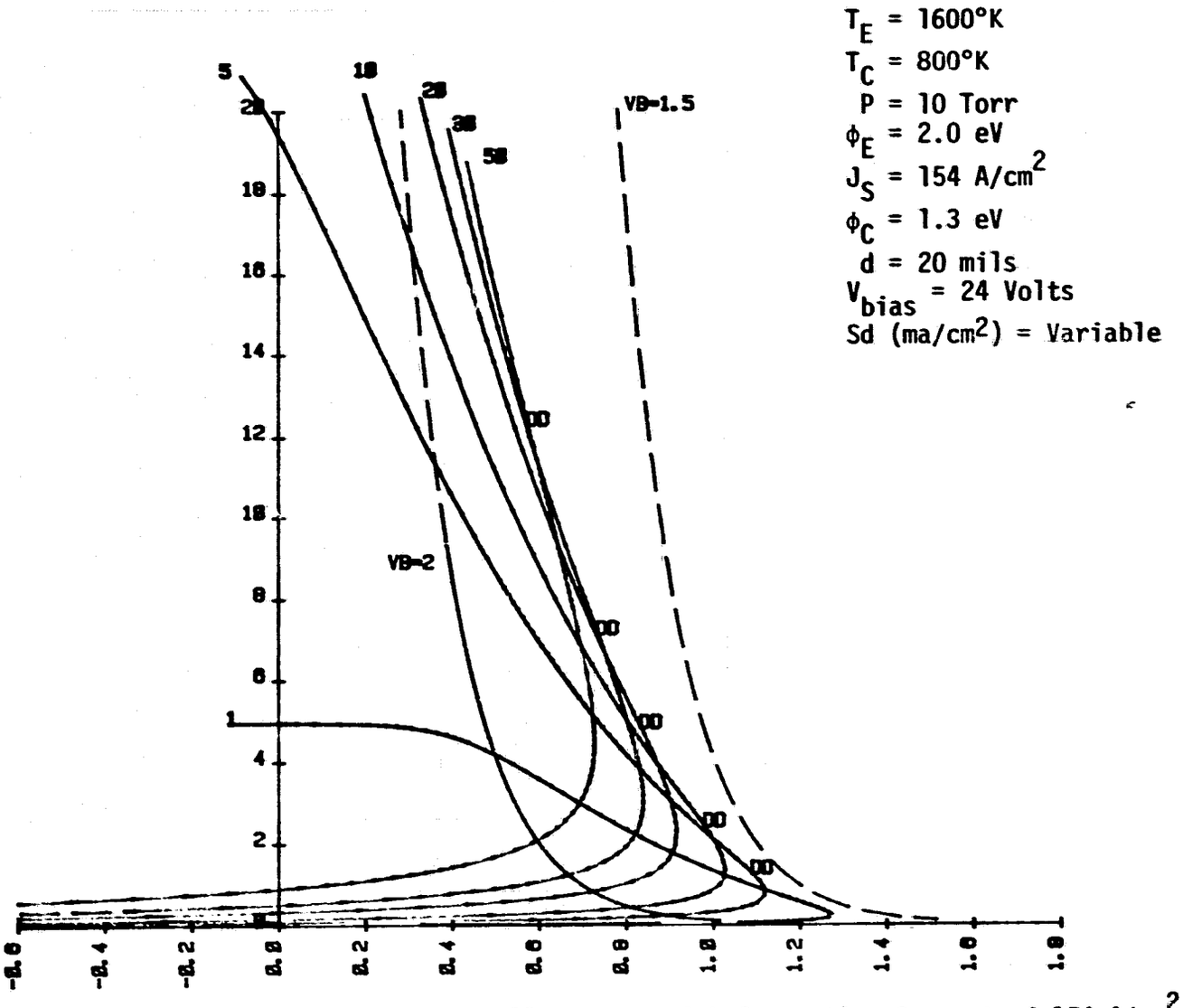

T_E = 1600°K
T_C = 800°K
P = 10 Torr
ϕ_E = 2.0 eV
J_S = 154 A/cm^2
ϕ_C = 1.3 eV
d = 20 mils
V_{bias} = 24 Volts
Sd (ma/cm^2) = Variable

Fig. 16 Calculated Performance of Xenon Plasmatron with Saturation Current of 154 A/cm^2

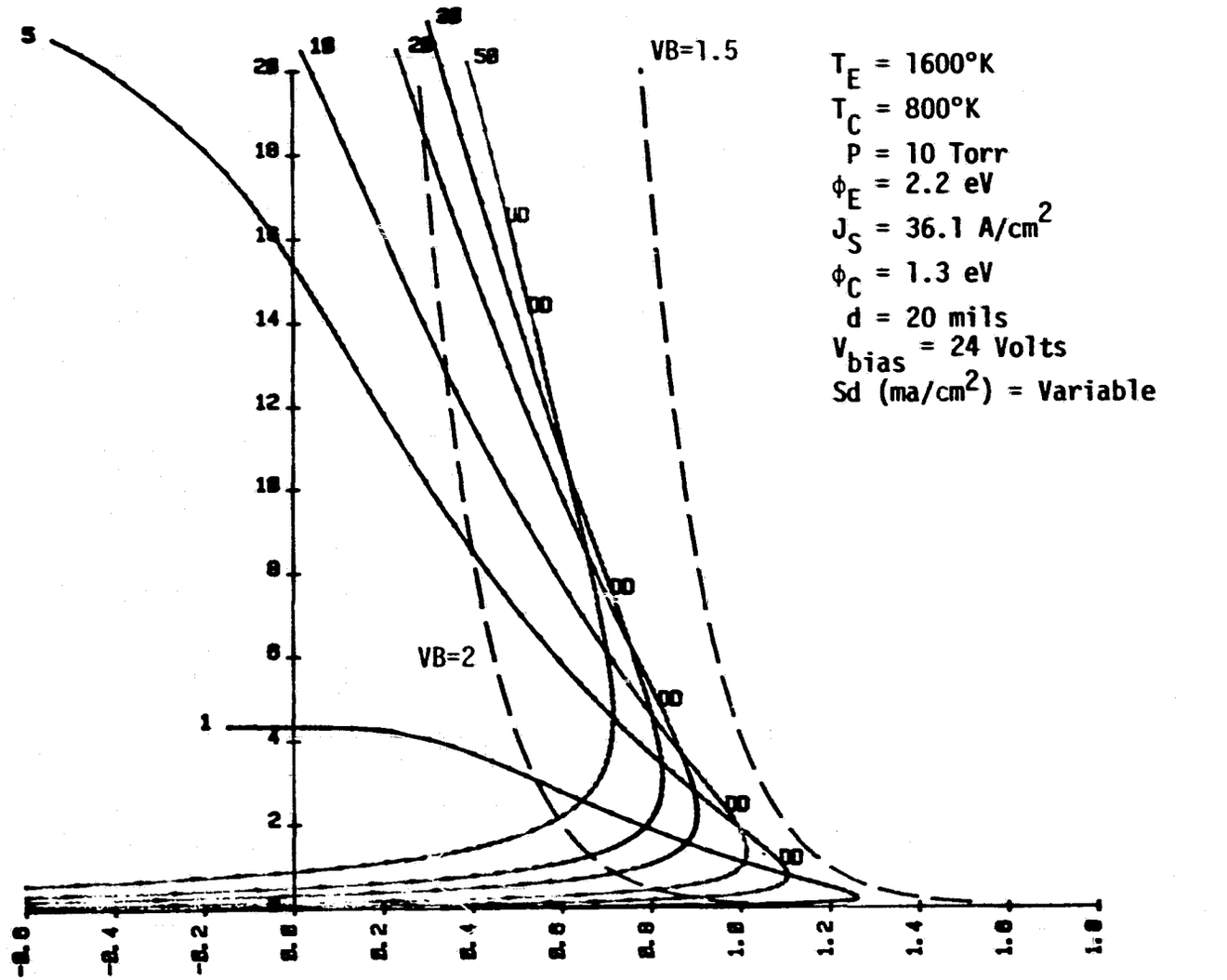

Fig. 17 Calculated Performance of Xenon Plasmatron with a Saturation Current of 36 A/cm^2

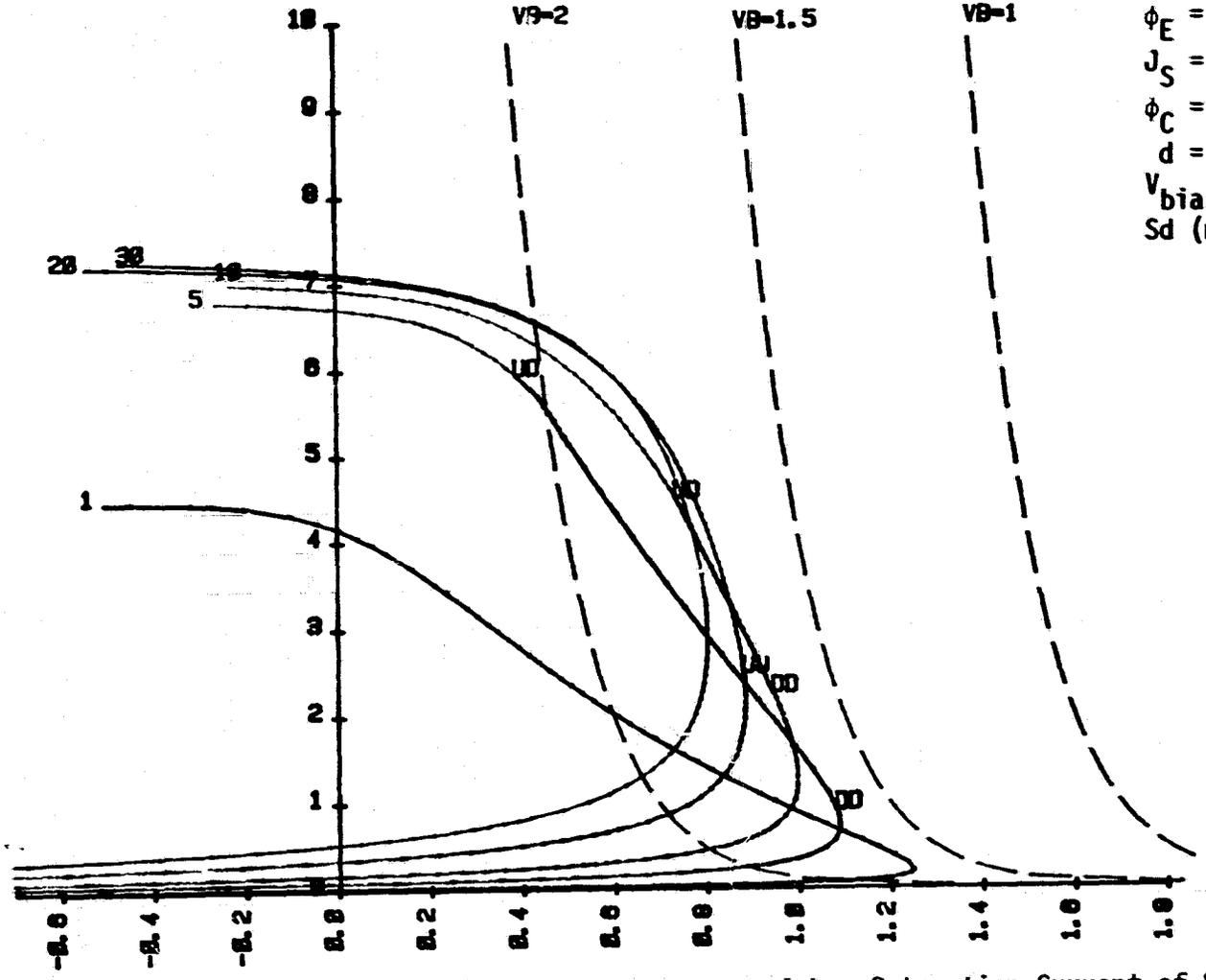

T_E = 1600°K
T_C = 800°K
P = 10 Torr
ϕ_E = 2.4 eV
J_S = 8.5 A/cm^2
ϕ_C = 1.3 eV
d = 28 mils
V_{bias} = 24 Volts
Sd (ma/cm^2) = Variable

Fig. 18 Calculated Performance of a Xenon Plasmatron with a Saturation Current of 8.5 A/cm^2

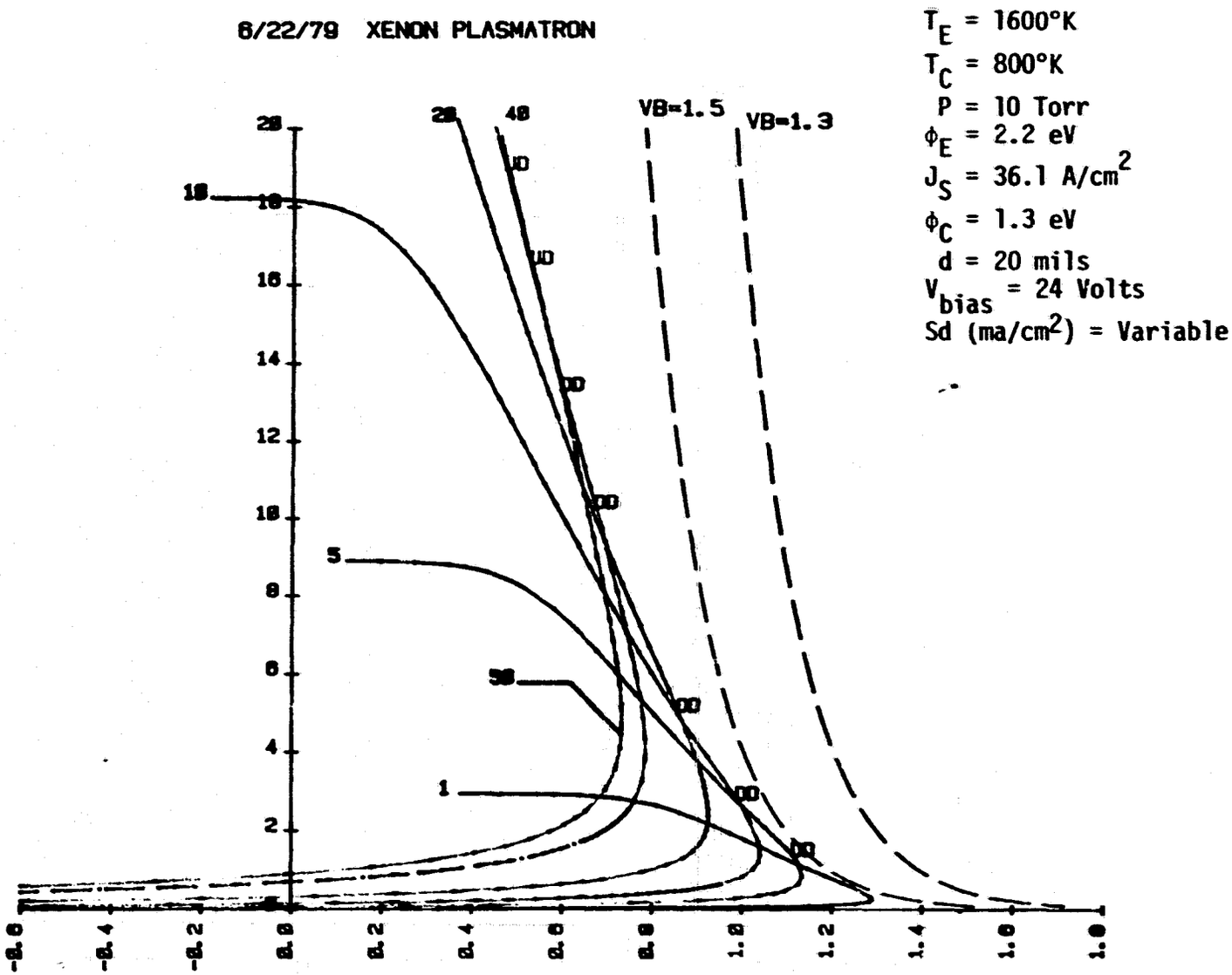

Fig. 19 Calculated Performance of a Xenon Plasmatron at 1 Torr

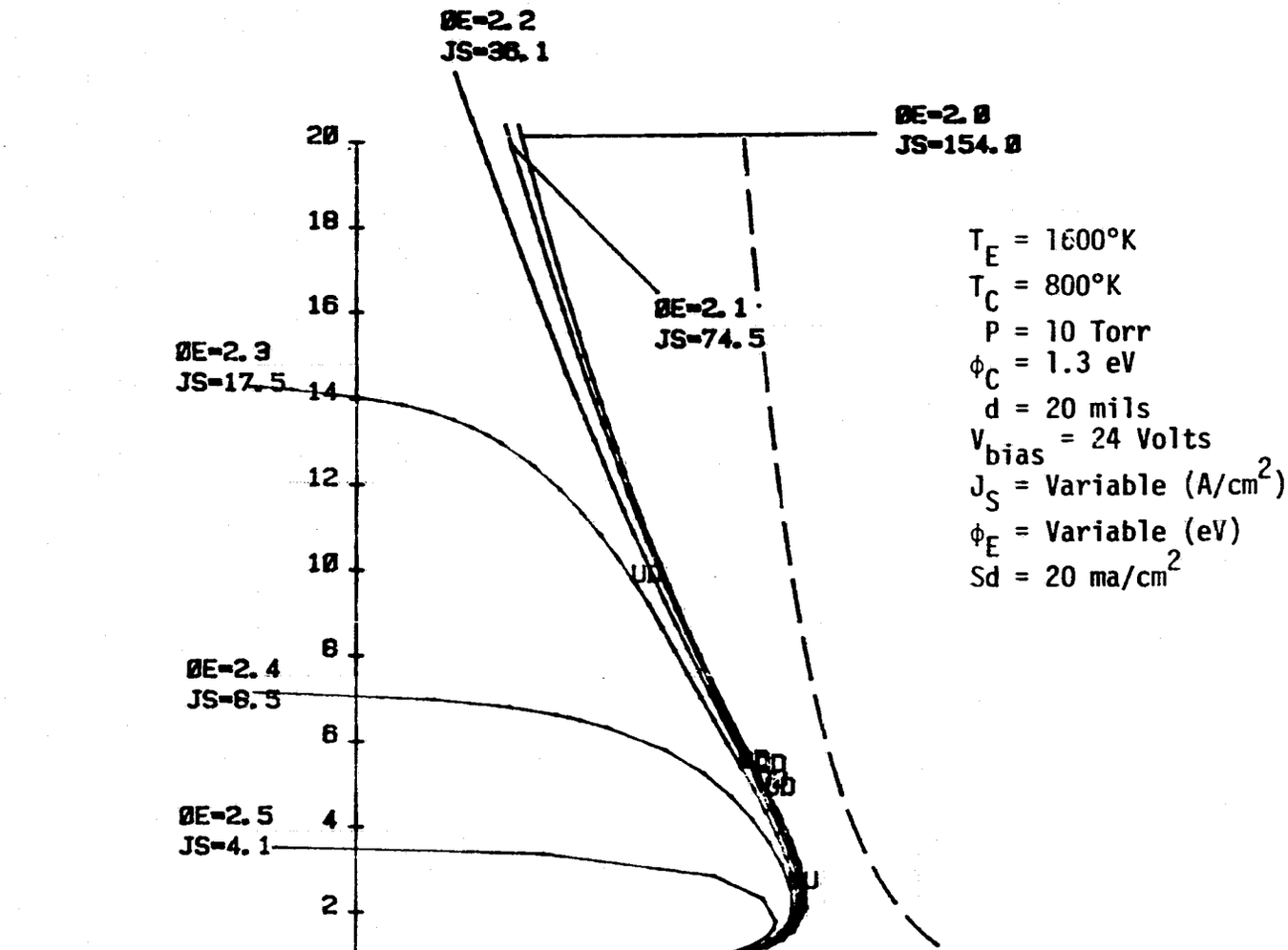

Fig. 20 Calculated Performance Effect of the Emitter Work Function in a Xenon Plasmatron

that attractive performance for the xenon plasmatron should be available if emitters with work functions of V_E = 2.2 to 2.3 eV can be found which are compatible with a moderate collector work function value of 1.3 eV.

Future work will better map the calculated performance of the plasmatron to predict the optimum operating point. The effect of structured electrodes will also be examined.

1.3.2 Plasma Characterization (G. L. Hatch)

Introduction: The objective of this task is to define theoretically and to determine experimentally the nature of the current and voltage losses associated with the interelectrode space and methods of reducing such losses. Earlier results in this program have shown the real advantages of using inert gases for the interelectrode plasma, as opposed to the cesium plasma used in conventional diodes. Particularly at low current densities (<2 A/cm^2) the use of inert gas and auxiliary ion sources can provide substantial reductions in the arc drop. They also permit the use of wider spacings, and lower temperatures for key components of the converter. The current effort addresses the problem of achieving this result at higher, more practical current densities (>5 A/cm^2). It also addresses the nature of the plasma-surface interface, particularly that of structured electrode surfaces.

Current Effort: Work during this reporting period concentrated on planning for activities during this contract period.

1.3.3 Electrode Surface Characterization (J.-L. Desplat, L. K. Hansen, H. Woo)

Introduction: The objective of this task is to develop and experimentally characterize the electrode surface systems required for successful and improved operation of converters in other tasks. Three approaches which could substantially improve performance are being studied. First, materials which can provide a low collector work function (<1.3eV) under converter operating conditions are being sought. A variety of materials with such work functions are available, but they do not perform well at collector temperatures or in the presence of cesium. Recently the work by J.-L. Desplat at NASA-Ames Research Center [14] has shown that a properly processed W-O surface stable

to 1250°K can have a cesiated work function below 1.0 eV. This appears to be a particularly attractive candidate for use in a converter.

Second, the development of emitter surface materials capable of operating a low cesium pressures are being developed. Operation at low cesium pressure permits wider electrode spacing, permits the use of otherwise unattractive collector surfaces, and permits the use of gases other than cesium for the interelectrode plasma. The recent development of W-Zr-C surfaces stable to 1800°K which have work functions near 2.6 eV has been very encouraging in this area.[15]

Finally, there is a real possibility that the use of very low work function collectors may result in the generation of negative ions at the collector surface. Such ions could eliminate the advantages of such low work function surfaces. Earlier work in this program has shown that both Cs^- and H^- are generated by such surfaces, but probably at a rate too low to offset performance gains. The possibility of cesium molecule complexes or converter contaminants forming harmful negative ions is under continuing study.

Two specific subtasks are in progress. The first is to study the characteristics of low work function surfaces in cesium vapor. This effort is being complemented with a joint program with NASA-Ames to study low work function surfaces under nonequilibrium conditions. The latter effort resulted in the discovery of the stable W-O surface last year. The second subtask is continuing the study of negative ion species using a special quadrupole mass spectrometer-converter test stand developed in FY1978.

Current Effort:

Surface Study (J.-L. Desplat): The initial equilibrium surface data on low work function surfaces will be obtained using a "Marchuk" tube. In this tube a plasma is created by igniting a discharge in a gas at low pressure (usually cesium vapor or a mixture of cesium vapor and a noble gas). The surface to be studied is immersed in this plasma and biased in such a way as to be surrounded by positive ions: it is then possible to study the electron emission from the surface without building up a repulsive electron space charge.

The Marchuk tube design adopted is shown in Fig. 21. The tube itself is built in Pyrex for economy and easiness of construction, but with stainless steel collars and flanges in order to be reusable. Oxide-free glass-metal bonds being very expensive, it was decided to use normal oxide-containing seals after a test of their resistance to Cs corrosion. (An alternate ceramic-metal design was prepared if the test was unsuccessful.) One Pyrex-SST seal was tested for a total of 420 h at temperatures between 150°C and 200°C (185 h alone at 200°C). The Cs kept its color inside the tube and after cleaning off the Cs, no leaks were found on the leak detector. The Cs attack on the Pyrex was considered minimal and the Marchuk tube was ordered from the supplier. The probe holders, the most sensitive components, are of the ceramic-metal type.

The cesium reservoir is a metal tube containing a breakable Cs ampoule. It can be isolated by a bakeable UHV valve, which makes it reusable and avoids cumbersome cesiation. The tube is connected through a bakeable valve to the UHV hardware necessary to pump down the experiment and introduce the required gases (oxygen and argon) inside the tube. A triode noble gas ion pump will be used in order to handle argon efficiently. A very simple design was adopted for the oven which is to be used for outgassing the tube and keeping its temperature above the Cs reservoir temperature: finned strip heaters heat by convection the air contained inside a well insulated box.

Negative Ion Study (L. K. Hansen, H. Woo): Past data on the quadrupole-converter experiment showed the existence of Cs^- and H^- ions in the thermionic converter and how these negative ion intensities depended on various converter parameters such as spacing, pressure, electrode temperature, and position on the volt-ampere curve. As interesting and suggestive as this data was, it was not conclusive in establishing the magnitudes and physical processses involved in the negative ion generation. Work on a number of modifications designed to provide better data continued during this period. While this work was in progress the possibility of residual hydrogen in a converter producing a space charge barrier at the collector was examined more carefully..

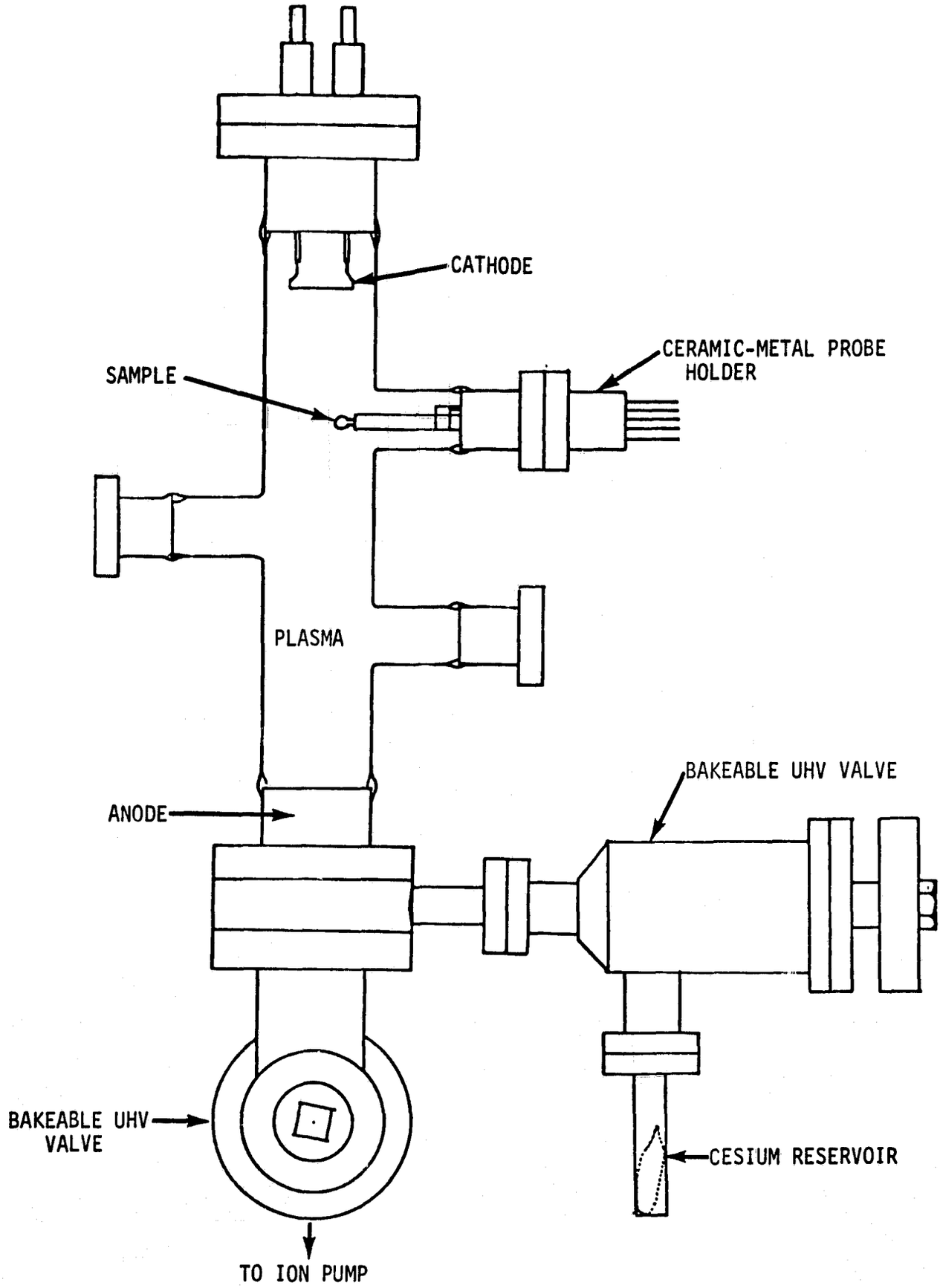

Fig. 21 Schematic Layout of the Plasma Anode Marchuk Tube Experiment

Data from the converter - quadrupole apparatus has shown large emission fluxes of negative hydrogen ions. These flux intensities were the same order as those for the cesium negative ions even though the cesium pressures were the order of 0.01 torr and the hydrogen pressure was merely that of the residual gas in the vacuum system, presumably about 10^{-5} torr.

A factor of 30-50 enhancement for the hydrogen over cesium can be explained with the Saha-Langmuir equation, because of the greater electron affinity of hydrogen (.75 eV versus .47 eV for Cs^-). Another factor of 5 in the hydrogen peak enhancement over cesium can be explained by the relative quadrupole transmission factors. The remaining factor of 4-100 difference must be explained by a superior secondary electron yield for hydrogen ions in the multiplier, an error in estimating the hydrogen pressure, or a real departure from the Saha-Langmuir equation.

Not much is known about secondary electron yields from negative ions, but presumably there is close to a 100% yield for both cesium and hydrogen.

It is very possible that there was an error in estimating the hydrogen partial pressure. This pressure could perhaps build up after the converter was isolated from the evacuation pump. On the one hand, it could be argued that the metal-to-ceramic seal members become permeable to hydrogen at their operating temperature, so that any out-gassed hydrogen would stay in equilibrium with the external vacuum which was the order of 10^{-5} torr. However, the cesium reservoir is also a strong source of hydrogen and may tend to keep the hydrogen partial pressure in equilibrium with itself rather than the external vacuum. Thus, the actual partial pressure of hydrogen in the converter is not known, even to an order of magnitude.

If we assume that the above discrepancy is due to a pressure estimation error and that the negative hydrogen ion yield is given by the Saha-Langmuir equation, then we can draw some conclusions about the possibility of hydrogen negative ions producing a space charge barrier at the collector.

The double sheath criterion for a surface with multiple negative ion emission is given by

$$1 = \frac{1}{2}\sqrt{\frac{\pi}{\eta}} + \left[\frac{\alpha}{2}(1+\Sigma_i R_i) - \frac{1}{2}\sqrt{\frac{\pi}{\eta}}\right]\exp(-\eta) \quad \text{(Ref. 16)} \tag{1}$$

where $$R_i = \frac{\nu_i}{\nu_e}\sqrt{\frac{M_i}{m}} \tag{2}$$

and where ν_i and ν_e are the ion and electron emission fluxes, M_i and m the ion and electron masses, α the fraction of the received electron flux from the plasma that is re-emitted thermally by the electrode, and η is the sheath height in units of kT_e where T_e is the electron temperature. The motive diagram is as follows

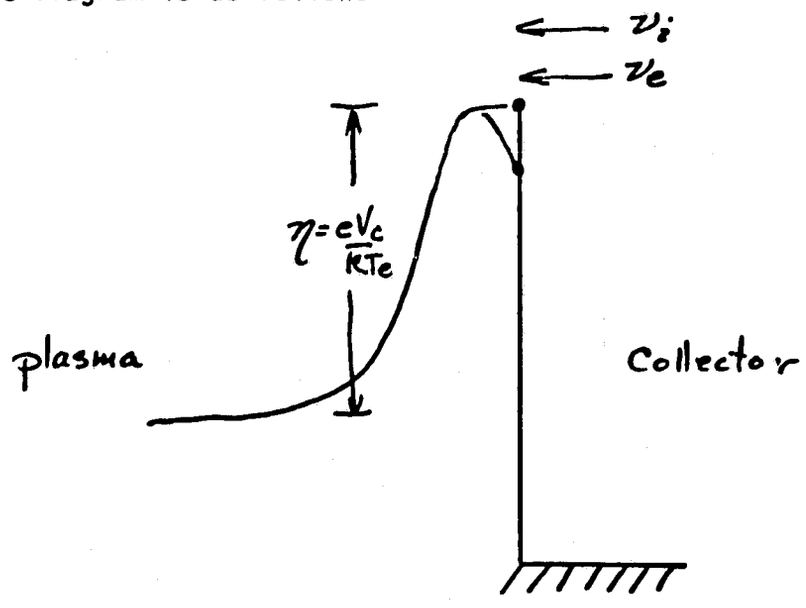

For hydrogen

$$R_i = \frac{\mu(H)e}{2A\,T_C^{\,2}} \exp\left(\frac{.75}{kT_C}\right)\sqrt{\frac{M_H}{m}} \tag{3}$$

where the arrival rate μ is given by

$$\mu(H) = \frac{p[\text{torr}]}{\sqrt{T_C[^\circ K]}} \times 3.503 \times 10^{21}\left[\frac{1}{cm^2\ sec}\right] \tag{4}$$

A is the Richardson constant $\left(120 \frac{\text{ampere}}{\text{cm}^2\ \text{deg}^2}\right)$, p is the hydrogen pressure and T_C is the temperature of the electrode (collector). The important point in determining the effectiveness of hydrogen in producing a space charge barrier is the magnitude of R_i in comparison to unity. Some typical values for R_i are shown in the table for p = 1 torr.

T_C	R_i (p = 1 torr)
400°K	8.76×10^4
500°K	6.47×10^2
600°K	22.53
700°K	1.93
800°K	.292
900°K	.065
1000°K	.019

If R_i is greater than unity, the thermal emission of the negative ion is more effective in producing a negative space charge barrier than electron emission. If less than unity, the electrons are more effective.

Since R_i is proportional to pressure, if the hydrogen partial pressure is the order of 10^{-3} torr or less, then for a typical converter ($T_C > T_R > 500°K$) the electron back emission from the collector is more effective in producing a space charge barrier. However, before this back emission produces a barrier it has reversed the flow of current and the electrode is no longer a collector. Thus the only way to get hydrogen to produce a space charge barrier by Saha-Langmuir emission is to raise the hydrogen pressure to very high values. As an example, by detailed plotting of Eq. 1 it was found that at T_C = 800°K, if back electron emission is half the forward plasma current, then a space charge barrier can be generated with the negative hydrogen ion emission only if the hydrogen pressure is raised to 5-10 torr. This conclusion is independent of the collector work function.

Incidentally, it should be noted that at equivalent arrival rates hydrogen is more effective than the monomer of cesium in causing a space charge effect. The ratio of effectiveness is given by

$$\frac{R_i(H)}{R_i(Cs)} \approx \sqrt{\frac{1}{133}} \exp\left(\frac{.28}{kT_C}\right), \tag{5}$$

or in the tabular form:

T_C	$R_i(H)/R_i(Cs)$
400°K	292.25
600°K	19.49
800°K	5.034
1000°K	2.234

Hydrogen, however, is normally at a much lower pressure than the cesium and therefore, under typical converter conditions, is less important than cesium in producing a negative space charge barrier.

There remains the possibility that some nonequilibrium process is responsible for the apparent high negative ion emission of hydrogen as observed by the quadrupole spectrometer. Whatever this possibility is, it can't effect the space charge at collector if the process involves the acceleration of positive ion through the collector sheath to the collector. If this positive ion current produced a high yield secondary negative ion emission the effect could at best cancel out the incoming positive ion space charge. Because of low hydrogen ion density the contribution of either the positive or negative hydrogen to the total positive ion space charge would be small compared to the cesium positive ion charge.

There remains only the possibility of a secondary ion effect due to hyperthermal neutral species or some chemical effects not yet postulated.

In summary, at this point of our understanding of collector phenomena, there appears to be no possible contribution of residual hydrogen to a negative space charge barrier at the collector.

1.3.4 Thermionic Converter Data Review (L. K. Hansen)

Introduction: Information on various aspects of converter physics or operation is widely dispersed in both published and unpublished form. Few single references exist which summarize this information. This task will begin the process of reviewing and summarizing this information in such a format that the result of previous work will be generally available.

Current Effort: An effort to acquire electron-neutral cesium cross-section data was begun.

TASK 2 - THX POWER MODULE EVALUATION

2.1.1 THX Test Module (L. L. Begg, B. Carlsmith)

Introduction: The overall objective of the THX Test Module Task is to provide a proper evaluation of the THX power module concept prior to a decision to develop prototype devices.

This evaluation will be made by designing, fabricating, and testing a preprototypic device. The modular nature of the THX permits such a realistic evaluation of the technology at minimum cost.

The preprototype THX will include all essential components, including heat transfer system (heat pipe), power output system and representative THX cells (both the end cells and a central cell). Since the THX consists of two end cells and a variable number of central cells, the development of this three cell module will be representative of THX modules with more than one central cell. The THX Test Module will be sized so as to permit evaluation for both central station power plant and industrial cogeneration applications.

During this current contract period effort will concentrate on designing the THX Test Module in sufficient detail to project probable performance, input power requirements, component operating temperatures and heat fluxes, materials, and required auxiliary test equipment. Supporting component tests, such as material strength or joint design, will be performed as needed to support the design effort.

Current Effort: The THX design computer code developed for system studies will be used to guide the THX Test Module design effort. Its projection of THX performance and cost will be used in combination with Test Module cost estimates and fabrication capability estimates to establish the Test Module design approach (inductive or series power coupling for example) size, and design operating point.

To facilitate the use of the code for this purpose it was modified during this period to compute THX performance and cost using series connected THX modules as well as inductively coupled module designs. Further modifications were made to permit generation of continuous parametric performance and cost plots as a function of such parameters as THX size, performance level, and operating point. Figs. 22 and 23 show illustrative results as a function of emitter temperature and current density for V_B = 1.5 and V_B = 1.0 for a variety of heat pipe diameters.

Future work will concentrate on extending the computer model to cover blade-type distributed leads. An effort to improve the modeling of TZM creep characteristics, a critical factor at temperatures above 1500°K, will begin shortly.

2.1.2 Heat Source (L. L. Begg, D. Johnson)

Introduction: The objective of this task is to provide the furnace facility required for development and operation of the THX Test Module.

Current Effort: No work was accomplished on this task during this reporting period.

2.1.3 Output Power Transfer System (L. L. Begg, E. J. Britt)

Introduction: The objective of this task is to provide the design, fabrication, and performance data needed to insure proper operation of the THX Test Module power transfer subsystem. Three possible subsystems are currently being considered: flux reset inductive power coupling, push-pull inductive power coupling, and series power coupling. The basic feasibility of inductive power coupling was demonstrated on a small scale early in this program, and series power coupling is the approach conventionally

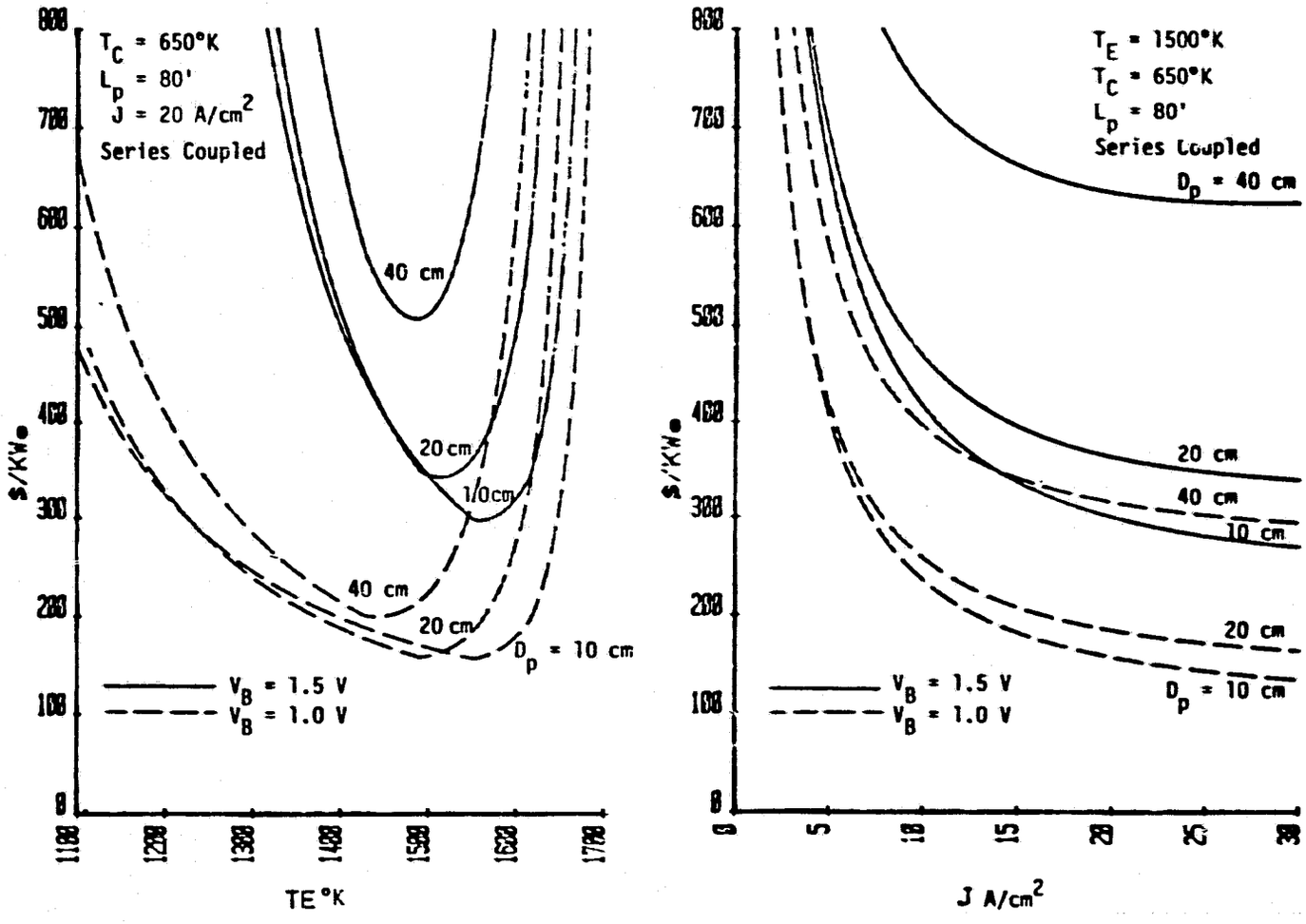

Fig. 22 The THX Design Program has been Upgraded to permit Parametric Optimization of Design Parameters. These illustrative Curves are for a Series Coupled Design.

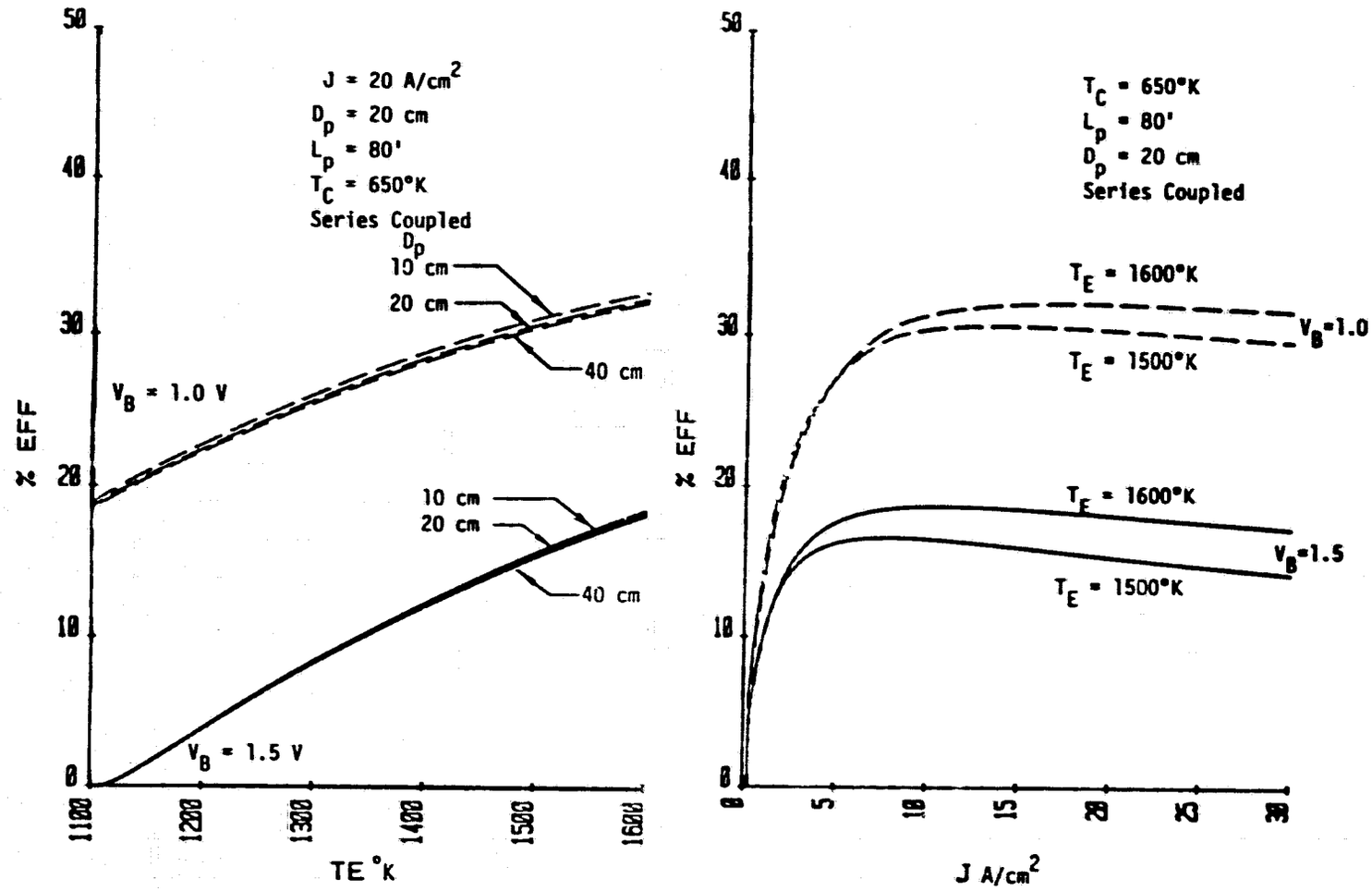

Fig. 23 The THX Design Program has been Upgraded to Permit Parametric Optimization of Design Parameters. These Illustrative Curves are for a Series Coupled Design.

used. The effort during this contracting period will concentrate on selecting one of these approaches for use in the THX Test Module. Following selection of the approach, a full scale engineering test will be accomplished at the currents and voltages typical of the THX Test Modules. The test will serve to confirm the early design methods and identify practical problem areas. Further tests will then be conducted to eliminate these problems. Finally a full scale test simulating actual THX power transfer conditions will be run in order to confirm the THX power system design and to obtain operating experience.

Current Effort: The NASA/JPL study of power coupling alternatives for the NEP thermionic power system showed that the converters in a reactor power system can be effectively connected in series to obtain high output voltages despite the fact that emitter heat pipes short out a portion of the output current.[17]

The computer program developed to analyze the NEP system was modified to consider a series connected THX array, as shown in Fig. 24. In this case the steam pipes which interconnect the THX power modules provide current leakage paths which result in higher current losses, I_x, as more modules are connected in series. Offsetting these current losses is a proportionately smaller power conditioning loss, V_s, as the output voltage of the series string of modules is increased. Fig. 25 shows the percentage of conditioned output power which is available as a function of the number of THX modules connected in series for a variety of steam pipe resistances. For comparison, a 3" O.D. steam pipe with a 1/4" wall, 3' long has a resistance of 0.75 milliohm. The use of such a pipe between the THX module and steam header in a series connected string of 14 modules would result in total power loss of only 13%, an encouraging result.

Further analysis of such series connected arrays will continue during the next report period.

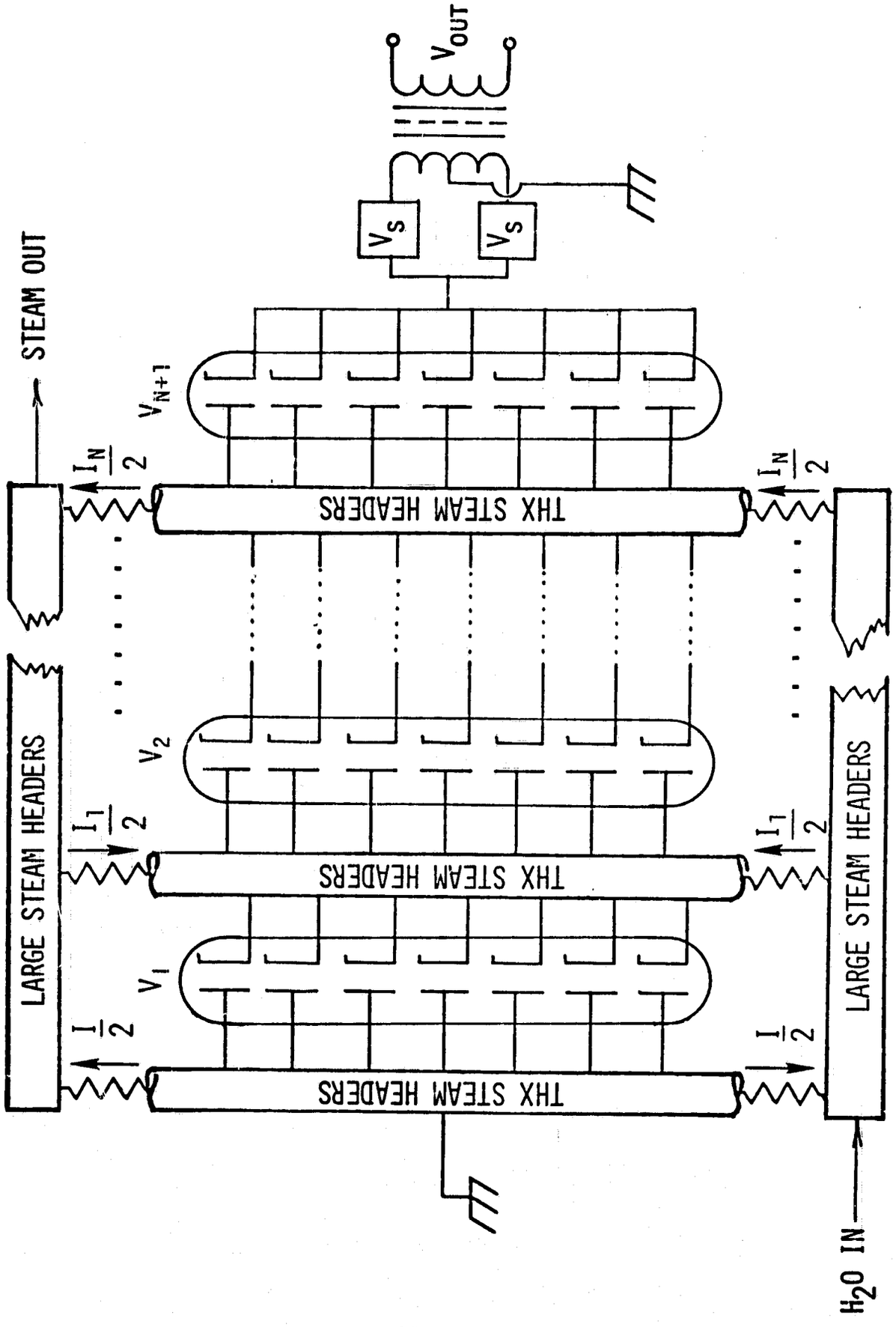

Fig. 24 Series Connected THX Array showing Leakage Current Paths

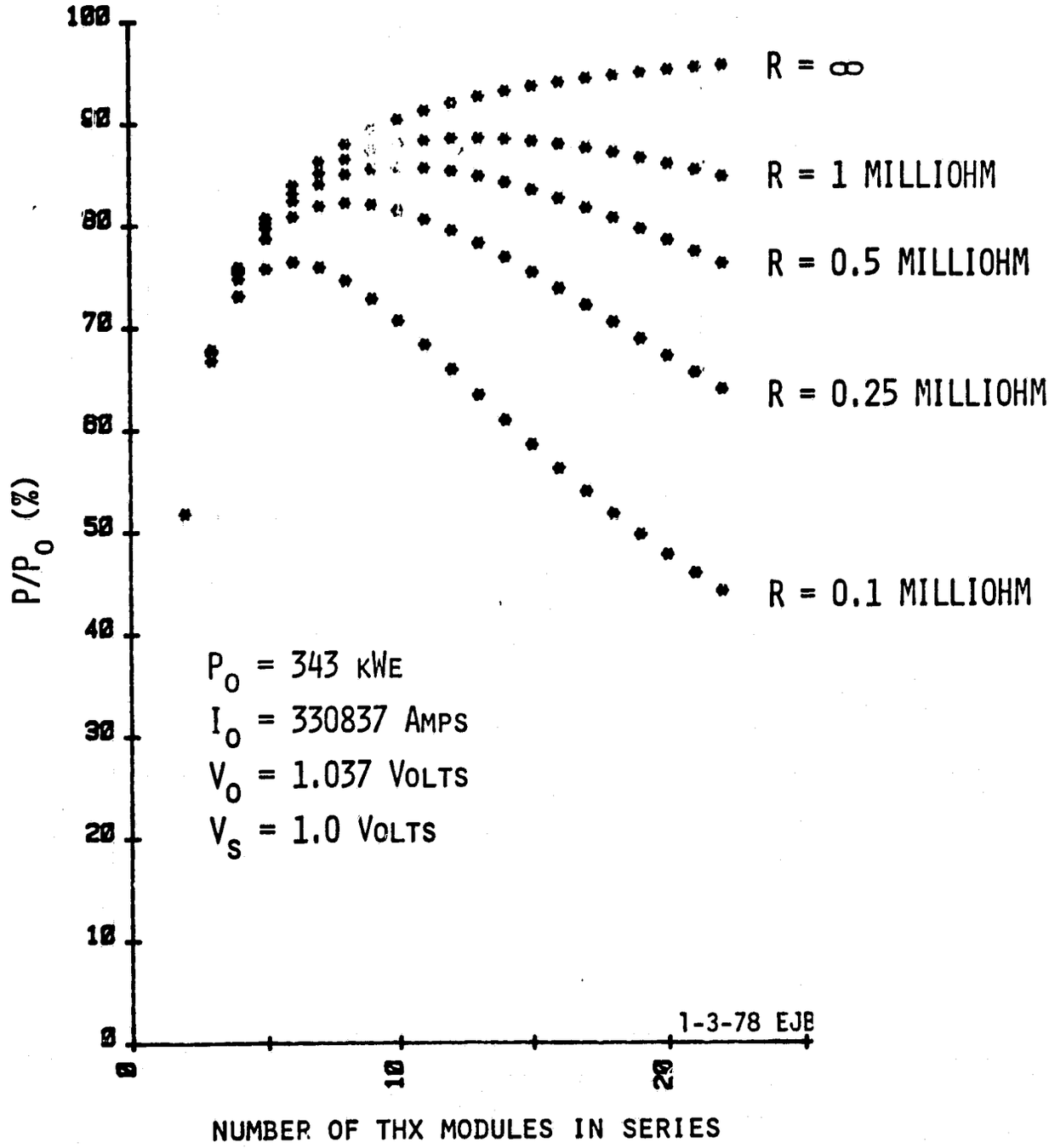

Fig. 25 Percentage of Available Output Power from a System of Series Connected THX Modules. Resistance of the Steam Pipes is Parametric.

2.1.4 Heat Transfer System (L. L. Begg)

Introduction: The objective of this task is to provide the design, fabrication, and performance data needed to ensure proper operation of the THX Power Module heat transfer system. The heat pipe which transfers thermal energy from the furnace to the THX module is a critical element of the module design. It must survive the combustion environment, transfer heat at high fluxes and temperatures, mate reliably to the power module, and provide a stable precision surface as an emitter substrate. This task will serve to establish the first two capabilities--combustion environment lifetimes and heat transfer capability--in heat pipe tests using the heat source facility. Supporting tests needed to establish the fabrication procedures, and define the heat pipe start up dynamics will be performed as necessary.

The effort during the current contract period will concentrate on defining the best heat pipe configuration (wick, arteries, structural supports, etc.) for use under THX operating conditions. Following definition of these aspects of the heat pipe design and initial results from the Heat Transfer Technology subtask (Task 1.1.2) a reference heat pipe design will be developed and fabrication processes established. A THX-scale heat pipe will then be built and tested at the heat flux and temperatures representative of THX operating conditions. Based on the results of this test recommendations will be made for modifications to the Reference THX Power Module Design.

Current Effort: A survey of heat pipe design literature was begun. Los Alamos has sent us their heat pipe design codes. The NASA "Heat Pipe Design Handbook," developed by Dynatherm, was also received.[18]

2.2 Conceptual Plant Design (G. O. Fitzpatrick, E. J. Britt)

Introduction: The objective of this task is to realistically define the performance potential of a coal-fired thermionic central station power plant. Preliminary system studies reported earlier in this program[4] have shown that combined thermionic-steam central station power plants can be both highly efficient and economic. However, these studies have been made assuming either relatively conventional power

plant components and steam cycles, or advanced components designed for other applications (such as an MHD type high temperature air preheater). The resources have not been available to fully optimize a thermionic power station, as opposed to a simple thermionic topping system. As a result the full potential of thermionics in the central station application has not been well defined. To provide such definition a more fully optimized design is being generated in three phases:

- Phase One - Baseline system definition and parametric analysis
- Phase Two - Conceptual plant design
- Phase Three - Development plan definition

In Phase One, which will be accomplished during the period of the current contract, a baseline coal-fired steam electric plant incorporating thermionic converters will be defined, and parametrically analyzed to determine, at a conceptual level of accuracy, the most economic process conditions and equipment designs. Data from this phase will provide the input for the conceptual design of a power plant equipped with thermionic converters in Phase Two. In addition it will provide initial estimates of system performance and major process component installed costs.

Based on the results of Phases One and Two, Phase Three will complete the study by recommending development goals for commercially acceptable thermionic converter systems for steam electric power plant applications.

The study is the joint effort of Rasor Associates, Inc., Bechtel National Corporation, and Foster Wheeler Development Corporation. The effort is divided between the participants as follows:

- Rasor Associates will provide overall coordination and required information pertaining to the performance, design and cost of the THX (Thermionic Heat Exchanger) modules.
- Foster Wheeler will provide required information pertaining to the performance, design and costs of coal-fired combustors equipped with thermionic converters.
- Bechtel will provide required information pertaining to the performance, design, environmental intrusion, capital costs,

construction schedule, and power generation economics of steam electric power plants equipped with the thermionic boilers as defined by Rasor Associates and Foster Wheeler.

Current Effort: Negotiations on work statements with Bechtel National, Inc. and the Foster Wheeler Development Corporation were begun.

PART II - NASA/JPL PROGRAM

TASK 1 - CONVERTER FABRICATION AND TEST (G. L. Hatch, M. L. Manda)

Introduction: The overall objective of this effort is to measure the operating efficiency of converters using the best available electrodes and operating modes. In 1978 this effort concentrated on establishing the design and fabrication procedures for a new cylindrical converter test vehicle specifically engineered to meet this need. Five such converters were built and tested, proving the effectiveness of the design. These five were used to study structured electrode effects. The test results indicated that structured surfaces could provide an output voltage increase of ~0.1 volt, with a concurrent improvement in efficiency below T_E ~1700°K. Above 1700°K efficiencies were not improved, probably because of increased radiation losses due to the higher emissivities of the structured surfaces. The best performance demonstrated at the design temperature of 1700°K was an efficiency of 12% with a lead power density of 2.6 W/cm^2. The converter providing this performance had a structured rhenium emitter and smooth molybdenum collector.

Beginning in March 1979, the specific objective of this task is to operate a converter with a lead efficiency of 15% and an output power density of 5 W/cm^2 at an emitter temperature, nominally 1650°K, suitable for application to a space nuclear power system. To achieve this objective three cylindrical converters will be built and operated.

Current Effort: During this period the life test of JPL-5 (STR/STR) converter has continued on test to establish the integrity of the converter envelope. No failure in the converter components or testing apparatus has been experienced. Plant power and water pressure failure have caused two unscheduled converter shutdowns but have not affected the converter performance. Each time testing was resumed without apparent harm to the converter envelope. Plans are being formulated to eliminate these interruptions from future tests. The converter's performance characteristics as shown by variable cesium family curves have been taken periodically. A decrease in converter output and efficiency of about 10% have been observed.

After approximately 1700 hours of continuous testing the converter was shutdown. After a month the converter was returned to life tests and to date has accumulated 2200 hours of operation.

Planning for the three cylindrical converters to be tested during this contract period was continued.

TASK 2 - UNINSULATED HEAT PIPE THERMIONIC POWER ANALYSIS (E. J. Britt)

Introduction: The objective of this task is to evaluate the possibility of using uninsulated converters in a nuclear space power system for application to electric propulsion. In the current system design a sheath insulator is used to electrically isolate the emitter of each converter in the power conversion array from the heat pipes which transport heat from the reactor core to the array. If the need for this insulator could be eliminated a difficult materials requirement would also be eliminated, permitting a broader choice of operating parameters (emitter temperature, etc.). During 1978 a review of a variety of techniques showed that the use of flux reset or push-pull power coupling was possible, although the latter would probably result in an excessively heavy system. The most attractive approach appears to be one with series coupled converters utilizing the electrical resistance of the heat pipes between the converter and the reactor core to minimize electrical losses.

During this contract period these systems will be examined parametrically following development of a converter performance code. The potential and advantages of the uninsulated system design will then be evaluated.

Current Activity: No work was accomplished on this task during this reporting period.

REFERENCES

1. "ZEPO - The Worlds Largest Thermionic Energy Converter," L. L. Begg and G. O. Fitzpatrick, presented at the 14th IECEC, August 1979.

2. "Advanced Thermionic Energy Conversion," Progress Report 9/74-8/75, COO-2263-4, NSR 2-4.

3. "Thermionic/Thermoelectric Energy Conversion Technology Development Program," Vol. 1 - Progress Report: October 1978 - January 1979 May 3, 1979, 730-49, Jet Propulsion Laboratory.

4. "Thermionic Power Plant Design Point Selection: The Economic Impact," G. O. Fitzpatrick and E. J. Britt, presented at the 13th IECEC, 1978.

5. "Design Study of a Coal-Fired Thermionic-Topped Power Plant Using an Advanced Boiler," G. Miskolczy and A. E. Margulies, presented at the 14th IECEC, 1979.

6. J. Morris, NASA Lewis Research Center, private communication.

7. "Advanced Thermionic Converter Development," F. N. Huffman et.al, presented at the 11th IECEC, Stateline, Nevada, September 1976.

8. "A Summary of USSR Thermionic Energy Conversion Acitivity," N. S. Rasor, presented at the IECEC, August 1978.

9. "Development of a Thermionic Reactor Space Power System, Final Summary Report," Gulf-GA-A12608, UC-33 Propulsion Systems and Energy Conversion, June 30, 1973.

10. "Advanced Thermionic Energy Conversion, Joint Highlights and Status Report," Rasor Associates, Inc., COO-2263-14, NSR 2-14, January-March 1979.

11. Werner Bloss, Doctoral Thesis, Technischen Hochschule Stuttgart, 1962; also Z. Angew, Phys. 14, 1 (1962); also Advanc. Energy Conv. 3 315 (1963).

12. Suso Weber, Doctoral Thesis, Technischen Hochschule Stuttgart, 1964.

13. Unpublished Paper Electron Transport Coefficients, Rapid Method of Evaluation, Princeton University Plasma Physics Laboratory, NJ, M. Stoenescu and P. Heinicke.

14. "A Study of Cesium Oxygen Coadsorption on Metallic Substrates," J.-L. Desplat, NSR 6-2, NASA CR-152272, May 1979.

15. "Fabrication and Surface Characterization of Composite Refractory Compounds Suitable for Thermionic Converters," L. W. Swanson and P. R. Davis, Progress Report No. 6: February 15, 1979, JPL Contract No. 955156.

16. "Negative Ions and the Collector Sheath in a Thermionic Converter," Lorin K. Hansen, Rasor Associates, Inc. NSR 2-9 (Aug. 1978).

17. "Power Coupling Alternatives for the NEP Thermionic Power System," M. L. Manda, E. J. Britt, G. O. Fitzpatrick, NSR 7-1, JPL Contract 955121, December 1978.

18. "Heat Pipe Design Handbook," Dynatherm Corporation, DRL-2, DRD No. SE-354T, DTM 72-3.

APPENDIX 1
THE AUXILIARY ION SOURCE ANALYTICAL MODEL "AIS-1"

I. Theoretical Description

The continuum equations used to describe the auxiliary ion source converter are

$$\vec{\Gamma}_e = -D_e \nabla n - \mu_e n \vec{E}, \tag{1}$$

$$\vec{\Gamma}_i = -D_i \nabla n + \mu_i n \vec{E}, \tag{2}$$

and

$$\nabla \cdot \vec{\Gamma}_e = \nabla \cdot \vec{\Gamma}_i = S, \tag{3}$$

where S is the auxiliary ion source term and, and is constant with space. Eliminating $\vec{E}$ from Eqs. (1) and (2) gives

$$\frac{\vec{\Gamma}_e}{\mu_e} + \frac{\vec{\Gamma}_i}{\mu_i} = -\left(\frac{D_e}{\mu_e} + \frac{D_i}{\mu_i}\right) \nabla n, \tag{4}$$

which can be rewritten as

$$-\frac{\mu_i \vec{\Gamma}_e + \mu_e \vec{\Gamma}_i}{\mu_i D_e + \mu_e D_i} = \nabla n . \tag{5}$$

Writing Eq. (5) in one dimension gives

$$-\frac{(\mu_i \Gamma_e + \mu_e \Gamma_i)}{\mu_i D_e + \mu_e D_i} = \frac{dn}{dx} . \tag{6}$$

Taking the derivative of both sides and ignoring the spatial dependence of the transport coefficients yields

$$\mu_i \frac{d\Gamma_e}{dx} + \mu_e \frac{d\Gamma_i}{dx} = -(\mu_i D_e + \mu_e D_i) \frac{d^2 n}{dx^2} . \tag{7}$$

Using Eq. (3) gives

$$S = -\left(\frac{\mu_i D_e + \mu_e D_i}{\mu_i + \mu_e}\right)\frac{d^2n}{dx^2} . \tag{8}$$

The ambipolar diffusion coefficient D_a is defined as

$$D_a = \frac{\mu_i D_e + \mu_e D_i}{\mu_i + \mu_e} . \tag{9}$$

Substituting this into Eq. (8), we have

$$S = -D_a \frac{d^2n}{dx^2} . \tag{10}$$

If S and D_a have no spatial dependence, then this is a second-order linear differential equation with constant coefficients, and can be solved analytically to yield n(x).

Rewriting Eq. (10), we have

$$\frac{d^2n}{dx^2} = -\frac{S}{D_a} . \tag{11}$$

Integrating and applying boundary conditions gives

$$\frac{dn}{dx} = -\frac{S}{D_a}x + \frac{dn}{dx}\Big|_o . \tag{12}$$

Integrating again yields

$$n(x) = -\frac{Sx^2}{2Da} + \left(\frac{dn}{dx}\Big|_o\right)x + n_E , \tag{13}$$

where

$$\frac{dn}{dx}\Big|_o = -\frac{(\mu_i \Gamma_{eE} + \mu_e \Gamma_{iE})}{\mu_i D_e + \mu_e D_i} \tag{14}$$

by Eq. (5).

The plasma voltage drop V_p can be found by first solving Eq. (1) for E;

$$\vec{E} = -\left(\frac{\vec{\Gamma}_e}{\mu_e}\frac{1}{n} + \frac{D_e}{\mu_e}\frac{\nabla n}{n}\right). \tag{15}$$

Using the Einstein relations,

$$\mu_e = \frac{eD_e}{kT_e} \tag{16}$$

and

$$\mu_i = \frac{eD_i}{kT_i} \tag{17}$$

where T_e and T_i are the average values of the electron and ion temperatures respectively *

gives

$$\vec{E} = -\left(\frac{\vec{\Gamma}_e}{\mu_e}\frac{1}{n} + \frac{kT_e}{e}\frac{\nabla n}{n}\right) = \nabla V. \tag{18}$$

Since $V_p = -V(d)$, Eq. (17) gives

$$\frac{eV_p}{kT_e} = \int_o^d \frac{\Gamma_e}{D_e}\cdot\frac{dx}{n(x)} + \int_o^d \frac{dn}{n}. \tag{19}$$

* Note: At the boundaries of the plasma $T_i = T_e$ on the emitter side, and $T_i = T_C$ on the collector side.

In discussing the boundary conditions, it will be convenient to introduce a shorthand notation:

UU - case of electron-retaining sheaths at both electrodes

DD - case of ion-retaining sheaths at both electrodes

DU - case of an ion-retaining sheath at the emiter and an electron-retaining sheath at the collector

UD - case of an electron-retaining sheath at the emitter and an ion-retaining sheath at the collector.

For the UU case the simplified boundary conditions are

$$\Gamma_{eE} = a_E \left[\frac{J_s}{e} - \left(\frac{n_E \, v_e}{4} \right) \zeta'_E \right], \tag{20}$$

$$\Gamma_{iE} = \frac{A_E}{A_p} \left[\frac{J_i}{e} \xi'_E - \frac{n_E \, v_i}{4} \right], \tag{21}$$

$$\Gamma_{eC} = a_C \left[\frac{n_C \, v_e}{4} \zeta'_C - \frac{J_C}{e} \right], \tag{22}$$

and

$$\Gamma_{iC} = \frac{A_C}{A_p} \frac{n_C \, v_i}{4} ; \tag{23}$$

where

$$\zeta'_E = \exp \left(- \frac{eV_E}{kT_e} \right), \tag{24}$$

$$\zeta'_C = \exp \left(- \frac{eV_C}{kT_e} \right), \tag{25}$$

$$\xi'_E = \exp \left(- \frac{eV_E}{kT_E} \right), \tag{26}$$

$J_s \equiv$ Richardson Current to the Emitter,

and $J_C \equiv$ Collector Back Emission Saturation Current.

Here $a_E = \frac{A_E}{A_P}(1-r_E)$, where $\frac{A_E}{A_P}$ is the ratio of the convoluted emitter surface to the projected surface of the plasma, and r_E is the quantum mechanical electron reflectivity of the emitter surface. Similarly for the collector, $a_C = \frac{A_C}{A_P}(1-r_C)$.

Conservation of current implies that

$$\Gamma_{iC} - \Gamma_{iE} = \Gamma_{eC} - \Gamma_{eE}. \tag{27}$$

Integrating Eq. (3) gives

$$\Gamma_{iC} - \Gamma_{iE} = \Gamma_{eC} - \Gamma_{eE} = Sd. \tag{28}$$

For the DD case, the boundary conditions are

$$\Gamma_{eE} = a_E\left[\frac{J_s}{e}\zeta_E - \frac{n_E v_e}{4}\right], \tag{29}$$

$$\Gamma_{iE} = \frac{A_E}{A_P}\left[\frac{J_i}{e} - \frac{n_E v_i}{4}\zeta_E\right], \tag{30}$$

$$\Gamma_{eC} = a_C\left[\frac{n_C v_e}{4} - J_C \zeta_C\right], \tag{31}$$

and

$$\Gamma_{iC} = \frac{A_C}{A_P}\left(\frac{n_C v_i}{4}\right)\zeta_C; \tag{32}$$

where

$$\zeta_E = \exp\left(-\frac{eV_E}{kT_E}\right). \tag{33}$$

and

$$\zeta_C = \exp\left(-\frac{eV_C}{kT_C}\right). \tag{34}$$

For the DU case

$$\Gamma_{eE} = a_E\left[\frac{J_s}{e}\zeta_E - \frac{n_E v_e}{4}\right], \tag{35}$$

$$\Gamma_{iE} = \frac{A_E}{A_p}\left[\frac{J_i}{e} - \left(\frac{n_E v_i}{4}\right)\zeta_E\right], \tag{36}$$

$$\Gamma_{eC} = a_C\left[\left(\frac{n_C v_e}{4}\right)\zeta'_C - \frac{J_C}{e}\right], \tag{37}$$

and

$$\Gamma_{iC} = \frac{A_C}{A_p}\left(\frac{n_C v_i}{4}\right). \tag{38}$$

Finally, the UD case boundary conditions are

$$\Gamma_{eE} = a_E\left[\frac{J_s}{e} - \left(\frac{n_E v_e}{4}\right)\zeta'_E\right], \tag{39}$$

$$\Gamma_{iE} = \frac{A_E}{A_p}\left[\frac{J_i}{e}\zeta'_E - \frac{n_E v_i}{4}\right], \tag{40}$$

$$\Gamma_{eC} = a_C\left[\frac{n_C v_e}{4} - \frac{J_C}{e}\zeta_C\right], \tag{41}$$

and

$$\Gamma_{iC} = \frac{A_C}{A_p}\left(\frac{n_C v_i}{4}\right)\zeta_C. \tag{42}$$

II. Solution of the Equations

Evaluating Eq. (13) for n(x) at x = d and rearranging gives

$$n_E = n_C + \frac{Sd^2}{2D_a} - \left(\frac{dn}{dx}\Big|_o\right) d. \tag{43}$$

Eq. (14) is substituted into Eq. (47) to give

$$n_E = n_C + \frac{Sd^2}{2D_a} + \left(\frac{\mu_i \Gamma_{eE} + \mu_e \Gamma_{iE}}{\mu_i D_e + \mu_e D_i}\right) d. \tag{44}$$

The diffusion coefficients and mobilities can be eliminated using the Einstein relations, Eqs. (16) and (17) and by

$$D_e = \frac{\lambda_e v_e}{3} \tag{45}$$

and

$$D_i = \frac{\lambda_i v_i}{3} \tag{46}$$

Here λ_e is the effective electron mean free path. It is a combination of the electron-neutral atom mean free path λ_{ea} and the coulombic mean free path λ_{ei};

$$\frac{1}{\lambda_e} = \frac{1}{\lambda_{ea}} + \frac{1}{\lambda_{ei}} . \tag{47}$$

The electron-neutral mean free path is evaluated by

$$\lambda_{ea} = \frac{1}{n_a \sigma_{ea}} \tag{48}$$

where n_a is the neutral atom density and σ_{ea} is the elastic collision cross section. This cross section is a function of electron temperature.

For the coulombic mean free path:

$$\lambda_{ei} = \frac{3\gamma_E (2\ kT_e)^{5/2}}{n v_e\ \pi^{3/2}\ m_e^{1/2}\ e^4\ \ln \Lambda} \tag{49}$$

where $\gamma_E = .582$ is a parameter which accounts for the effect of electron-electron interaction, and $\ln \Lambda$ is the coulomb logorithm.

Using Eqs. (45), (46), (16), (17), and Eq. (9), Eq. (44) becomes

$$n_E = n_C + \frac{Sd^2}{2}\ \frac{3(\alpha\lambda_e + r\lambda_i)}{v_e \lambda_e \lambda_i (r+1)}$$

$$+ \frac{3d}{(r+1) v_e \lambda_e}\left[r\Gamma_{eE} + \alpha\left(\frac{\lambda_e}{\lambda_i}\right)\Gamma_{iE}\right], \tag{50}$$

where

$$r = \frac{<T_e>}{<T_i>} \tag{51}$$

and

$$\alpha = \frac{v_e}{v_i}. \tag{52}$$

Using Eq. (28), Eq. (50) becomes

$$n_E = n_C - \frac{Sd^2}{2}\ \frac{3(\alpha\lambda_e + r\lambda_i)}{v_e \lambda_e \lambda_i (r+1)}$$

$$+ \frac{3d}{(r+1) v_e \lambda_e}\left[r\Gamma_{eC} + \alpha\left(\frac{\lambda_e}{\lambda_i}\right)\Gamma_{iC}\right]. \tag{53}$$

The solution must now involve the specific boundary conditions (UU, DD, DU, or UD). In general, the boundary conditions for Γ_{eC} and Γ_{iC} are used to eliminate n_C and Γ_{iC} in Eq. (53). Then the boundary condition for Γ_{eE} is used along with Eq. (28) to eliminate n_E. This results in a relation of the form

$$\Gamma_{eC} = f\left[\zeta_E(\text{or } \zeta_E'),\ \zeta_C(\text{or } \zeta_C')\right] \tag{54}$$

At this point it is convenient to introduce the following quantities:

$$E \equiv \frac{3}{4}\left(\frac{r}{r+1}\right)\frac{d}{\lambda_e} \tag{55}$$

and

$$I \equiv \frac{3}{4}\left(\frac{1}{r+1}\right)\frac{d}{\lambda_i} \tag{56}$$

The boundary conditions, together with Eq. (28) can be manipulated to find a relationship between the sheath factors:

$$\zeta_C(\text{or } \zeta_C') = g\left[\zeta_E(\text{or } \zeta_E')\right]. \tag{57}$$

This relationship is now used to eliminate ζ_C (or ζ_C') from Eq. (54) and form an equation for ζ_E in terms of only known quantities. These are tested together with the various forms of Eq. (57) for each boundary condition case.

For UU:

$$A\,\zeta_E'^{\,(T_e/T_E\,+\,1)} + B\,\zeta_E' + C = 0 \tag{58}$$

where

$$A = \frac{J_i}{J_s}\,\frac{A_E}{A_P}\,\alpha\left(\frac{A_P}{A_C} + I\right) \tag{59}$$

$$B = \frac{eSd}{2J_s}\left(2\,\alpha\,\frac{A_P}{A_C} + \alpha\,I - E\right) + \frac{e\Gamma_{eC}}{J_s} \tag{60}$$

$$C = \left[\frac{e(J_{eC} - Sd)}{A_E\,J_s} - 1\right]\left[1 + \frac{A_E}{A_P}\left(\frac{A_P}{A_C} + I\right)\right] \tag{61}$$

and

$$\frac{1}{\zeta_C'} = \left[\frac{A_E}{A_P}\left(\frac{e\Gamma_{eC}}{a_E} - \frac{eSd}{a_e} - J_s\right)\frac{1}{\zeta_E'} + \alpha\left(eSd + \frac{A_E}{A_P} J_i\ \zeta_E'\right)\right]$$

$$\frac{A_C}{A_P}\left(\frac{e\Gamma_{eC}}{a_C} + J_C\right) \tag{62}$$

For DD:

$$A\ \zeta_E^2 + B\ \zeta_E + C = 0 \tag{63}$$

where

$$A = \frac{A_E}{A_P} I, \tag{64}$$

$$B = \left(\frac{eSd - e\Gamma_{eC}}{J_s}\right)\frac{I}{(1-r_E)} + 1, \tag{65}$$

$$C = \frac{eSd}{2J_s}\left(\frac{2}{a_E} + E - \alpha I\right) \tag{66}$$

$$- \frac{e\Gamma_{eC}}{J_s}\left(\frac{1}{a_E} + \frac{1}{a_C} + E\right) - \frac{J_C\zeta_C}{J_s}$$

$$- \alpha I\ \frac{J_i}{J_s}\frac{A_E}{A_P},$$

and

$$\zeta_C = \left[\frac{A_C}{A_P}\left(\frac{e\Gamma_{eC}}{a_C} + J_C\zeta_C\right)\right]^{-1}\left[\frac{A_E}{A_P}\frac{(e\Gamma_{eC} - Sd)}{a_E}\zeta_E - J_s\frac{A_E}{A_P}\zeta_E^2\right.$$

$$\left.\alpha\left(Sd + J_i\frac{A_E}{A_P}\right)\right]. \tag{67}$$

For DU

$$A\,\zeta_E^2 + B\,\zeta_E + C = 0 \tag{68}$$

where

$$A = \left(\frac{A_E}{A_C} + I\,\frac{A_E}{A_P}\right), \tag{69}$$

$$B = \frac{1}{(1-r_E)}\,\frac{e(Sd - \Gamma_{eC})}{J_s}\left(\frac{A_P}{A_C} + I\right) + 1, \tag{70}$$

$$C = \frac{eSd}{2J_s}\left(\frac{2}{a_E} + E - \alpha I - 2\alpha\,\frac{A_P}{A_C}\right)$$

$$- \frac{e\Gamma_{eC}}{J_s}\left(\frac{1}{a_E} + E\right) - \frac{J_i}{J_s}\alpha\left(\frac{A_E}{A_C} + \frac{A_E}{A_P}\,I\right); \tag{71}$$

and

$$\frac{1}{\zeta_C} = \left[\frac{A_C}{A_P}\left(\frac{e\Gamma_{eC}}{a_C} + J_C\right)\right]^{-1}\left[\frac{A_E}{A_P}\left(\frac{e\Gamma_{eC}}{a_E} - \frac{eSd}{a_E}\right)\zeta_E\right.$$

$$\left. - \frac{A_E}{A_P}\,J_s\zeta_E^2 + \alpha\left(Sd + J_i\,\frac{A_E}{A_P}\right)\right]. \tag{72}$$

For UD:

$$A\,\zeta_E^{(T_e/T_E+1)} + B\,\zeta_E + C = 0 \tag{73}$$

where

$$A = \frac{A_E}{A_P}\,\alpha I\,\frac{J_i}{J_s}, \tag{74}$$

$$B = \frac{e\Gamma_{eC}}{J_s}\left(\frac{1}{a_C} + E\right) - \frac{eSd}{2J_s}\,(E - \alpha I) + \frac{J_C}{J_s}\,\zeta_C, \tag{75}$$

$$C = \left(1 + \frac{A_E}{A_P} I\right)\left(\frac{e}{J_s a_E}\Gamma_{eC} - \frac{eSd}{J_s a_E} - 1\right); \tag{76}$$

and

$$\zeta_C = \left[\frac{A_E}{A_P}\left(\frac{e\Gamma_{eC}}{a_E} - \frac{eSd}{a_E} - J_s\right)\frac{1}{\zeta_E'} + \alpha\, Sd + \frac{A_E}{A_P}\alpha\, J_i\, \xi_E'\right]\left[\frac{A_C}{A_P}\left(\frac{e\Gamma_{eC}}{a_C} + J_C\zeta_C\right)\right]^{-1} \tag{77}$$

The integral of Eq. (19) can be evaluated to give V_P. The equation gives

$$\frac{eV_P}{kT_e} = \int_0^{d_{\Gamma_e}} \frac{dx}{D_e}\frac{dx}{n} - \ell n\left(\frac{n_E}{n_C}\right) \tag{78}$$

The first term in the expression can be evaluated. From Eq. (13)

$$n(x) = a + b + c\, x^2 \tag{79}$$

where

$$a = n_E,$$

$$b = \frac{-(\mu_i\, \Gamma_{eE} + \mu_e\, \Gamma_{iE})}{\mu_i\, D_e + \mu_e\, D_i},$$

and

$$c = \frac{-S}{2Da}. \tag{80}$$

Solving Eq. (3) in one dimension with S constant gives

$$\Gamma_e = \Gamma_{eE} + Sx. \tag{81}$$

From Eqs. (45) and (47)

$$D_e = \frac{\lambda_e v_e}{3} = \frac{v_e}{3}\left(\frac{1}{\lambda_{ea}} + \frac{1}{\lambda_{ei}}\right)^{-1} \tag{82}$$

Using Eqs. (48) and (49) gives

$$D_e = (\delta n_a + \beta n)^{-1} \tag{83}$$

where $$\delta = \frac{3\sigma_{ea}}{v_e} \tag{84}$$

and $$\beta = \frac{\pi^{3/2}\, m^{1/2}\, e^4\, \ell n\, \Lambda}{\gamma_E (2\, kT_e)^{3/2}} \tag{85}$$

If $n_a(x)$ is approximated by a linear function, Eq. (83) becomes

$$D_e = (\delta_0 + \delta_1\, x + \beta n)^{-1} \tag{86}$$

where

$$\delta_0 = \frac{3\sigma_{ea}}{v_e}\, n_a(o) \tag{87}$$

and

$$\delta_1 = \frac{3\sigma_{ea}}{v_e}\left(\frac{n_a(d) - n_a(o)}{d}\right) \tag{88}$$

Using Eqs. (81) and (86), the integral becomes

$$\int_o^d \frac{\Gamma_e}{D_e}\frac{dx}{n} = \int_o^d \frac{(\Gamma_{eE} + Sx)(\delta_0 + \delta_1\, x + \beta n)}{n}\, dx \tag{89}$$

This can be rewritten as

$$\int_o^d \frac{\Gamma_e}{D_e}\frac{dx}{n} = \int_o^d \frac{(\Gamma_{eE} + S_x)(\delta_0 + \delta_1\, x)}{n}\, dx + \int_o^d \beta(\Gamma_{eE} + Sx)\, dx \tag{90}$$

$$= \int_o^d \frac{(\Gamma_{eE} + Sx)(\delta_0 + \delta_1\, x)}{n}\, dx + \beta\, \Gamma_{eE}\, d + \frac{\beta\, Sd^2}{2} \tag{91}$$

Using Eq. (79) gives

$$\int_o^d \frac{\Gamma_e}{D_e}\frac{dx}{n} = \int_o^d \frac{(\Gamma_{eE} + Sx)(\delta_0 + \delta_1 x)}{a + b x^2 + c x^2} dx + \beta \Gamma_{eE} d$$

$$+ \beta \frac{Sd^2}{2} \tag{92}$$

This integral is solved to give

$$\int_o^d \frac{\Gamma_e}{D_e}\frac{dx}{n} = \left(\delta_o \Gamma_{eE} - \frac{\delta_0 Sb}{2c} - \frac{\delta_1 \Gamma_{eE} b}{2c}\right.$$

$$\left. + \frac{\delta_1 Sb^2}{2c^2} - \frac{\delta_1 Sa}{c}\right)\frac{1}{\sqrt{b^2 - 4ac}}$$

$$\left[\ln\left(\frac{2cd(b + \sqrt{b^2 - 4ac}) + 4ac}{2D(b - \sqrt{b^2 - 4ac}) + 4ac}\right)\right]$$

$$+ \left(\frac{\delta_0 S}{2c} + \frac{\delta_1 \Gamma_{eE}}{2c} - \frac{\delta_1 Sb}{2c^2}\right) \ln\left(1 + \frac{bd + cd^2}{a}\right)$$

$$+ \frac{\delta_1 Sd}{c} + \frac{\beta Sd^2}{2} + \beta \Gamma_{eE} d \tag{93}$$

The values of Γ_{eE}, Γ_{iE}, and n_E in the parameters B and A can be evaluated using the boundary conditions and Eq. (28). This evaluation will depend on the sheath condition.

The electron temperature T_e can be calculated by an energy balance equation. It will be convenient to introduce the notation:

$$V^D_{E,C} = \begin{cases} 0 \text{ if the sheath is "up"} \\ V_{E,C} \text{ if the sheath is "down"} \end{cases}$$

and

$$V^U_{E'C} = \begin{cases} 0 \text{ is the sheath is "down"} \\ V_{E,C} \text{ if the sheath is "up".} \end{cases}$$

And also

$$J_S\text{eff} = \begin{cases} J_S \text{ if emitter sheath is "up"} \\ J_S\zeta_E \text{ if emitter sheath is "down",} \end{cases}$$

$$J_C\text{eff} = \begin{cases} J_C \text{ if collector sheath is "up"} \\ J_C\zeta_C \text{ if collector sheath is "down",} \end{cases}$$

and

$$J_i\text{eff} = \begin{cases} J_i \text{ if emitter sheath is "down"} \\ J_i\zeta_E' \text{ if emitter sheath is "up".} \end{cases}$$

The energy carried by electrons from the emitter into the plasma is

$$E_1 = a_E J_S\text{eff} (\phi_E + V^D_E + 2\frac{k}{e} T_E). \tag{94}$$

The electron energy lost by the plasma to the emitter is

$$E_2 = (a_E J_S\text{eff} - e\Gamma_{eE}) (\phi_E + V^D_E + 2\frac{k}{e} T_e). \tag{95}$$

The electron energy loss at the collector is

$$E_3 = (e\Gamma_{eC} + a_C J_C\text{eff}) (\phi_C + V^D_C + V_o + 2\frac{k}{e} T_e). \tag{96}$$

The energy input due to back emission is

$$E_4 = a_C J_C\text{eff} (\phi_C + V^D_C + V_o + 2\frac{k}{e} T_C) \tag{97}$$

The energy carried by ions from the plasma to the emitter can be written

$$E_5 = \left(\frac{A_E}{A_p} J_i\text{eff} - e\Gamma_{iE}\right)\left(\phi_{iE} + V_E^U + 2\frac{k}{e}T_i(0)\right). \tag{98}$$

The energy input from the emitter due to returning atoms is

$$E_6 = \left(\frac{A_E}{A_p} J_i\text{eff} - e\Gamma_{iE}\right)\left(\phi_{iE} - V_i + \phi_E + 2\frac{k}{e}T_E\right). \tag{99}$$

And that due to emitted ions is

$$E_7 = \frac{A_E}{A_p} J_i\text{eff}\ (\phi_{iE} + V_E^U + 2\frac{k}{e}T_E). \tag{100}$$

These terms (E_5, E_6, and E_7) can be combined to give the net energy gain at the emitter due to ions and atoms:

$$E_{iaE} = \frac{A_E}{A_p} J_i\text{eff}\ (\phi_a + 2\frac{k}{e}T_E)$$

$$- e\Gamma_{iE}\ (\phi_E - V_i - V_E^U)$$

$$(\phi_a = \phi_E + \phi_{iE} - V_i). \tag{101}$$

Using Eq. (28) this becomes

$$E_{iaE} = \frac{A_E}{A_p} J_i\text{eff}\ (\phi_a + 2\frac{k}{e}T_E)$$

$$- e\Gamma_{iC}\ (\phi_E - V_i - V_E^U)$$

$$+ eSd\ (\phi_E - V_i - V_E^U). \tag{102}$$

The energy loss at the collector due to ions is

$$E_8 = e\Gamma_{iC} \left(V_C^U + V_d + \phi_{iE} + 2\frac{k}{e} T_i(d)\right) \tag{103}$$

wher V_d is the arc drop.

Energy gained at the collector by returning atoms is

$$E_9 = e\Gamma_{iC} \left(\phi_{iE} + V_d + \phi_C + V_o - V_i + 2\frac{k}{e} T_C\right) \tag{104}$$

Eqs. (103) and (104) can be combined to give

$$E_{iaC} = e\Gamma_{iC} \left(V_o + \phi_C - V_C^U - V_i\right) . \tag{105}$$

The energy carried into the plasma by the auxiliary ion source current is

$$E_{10} = eSd \left(V_i + 2\frac{k}{e} T_i\right) \tag{106}$$

Combining Eqs. (102), (105), and (106) gives

$$E_{ia} = E_{iaE} + E_{iaC} + E_{10} \tag{107}$$

or

$$E_{ia} = \frac{A_E}{A_P} J_i eff \left(\phi_a + 2\frac{k}{e} T_E\right)$$

$$+ eSd \left(\phi_E - V_E^U + 2\frac{k}{e} T_i\right)$$

$$+ e\Gamma_{iC} \left(V_E^U - V_C^U - V_d\right). \tag{108}$$

The total energy gained by the plasma is

$$G = E_1 + E_4 + E_{ia}, \tag{109}$$

and the energy loss is

$$L = E_2 + E_3. \tag{110}$$

The electron temperature T_e is iteratively adjusted until

$$G \simeq L. \tag{111}$$